AN *IN VITRO* MODEL OF SENTINEL LYMPH NODES FOR ASSESSING THE EFFECTIVENESS OF MAGNETIC HYPERTHERMIA

By

Nguyen (Peter) Truong

B.Sc., Siena College, 2014

Loudonville, New York

A Thesis

Presented to Ryerson University

In Partial Fulfillment of the

Requirements for the Degree of

Master of Science

In the Program of

Biomedical Physics

Toronto, Ontario, Canada, 2016

Author’s Declaration

I hereby declare that I am the sole author of this thesis. This is a true copy of the thesis, including any required final revisions, as accepted by my examiners.

I authorize Ryerson University to lend this thesis to other institutions or individuals for the purpose of scholarly research.

I further authorize Ryerson University to reproduce this thesis by photocopying or by other means, in total or in part, at the request of other institutions or individuals for the purpose of scholarly research.

I understand that my thesis may be made electronically available to the public.

Peter Truong

Abstract

An *In Vitro* Model of Sentinel Lymph Nodes for

Assessing the Effectiveness of Magnetic Hyperthermia

Nguyen Truong

Master of Science, Biomedical Physics

Ryerson University, 2016.

Metastasis, the migration of tumor cells, occupies the lymphatic system via populating inside lymph nodes and forming secondary tumors. Hyperthermia is a treatment modality that eradicates cancer cells based on the denaturation of proteins and plasma cell membrane at temperatures above 40 °C. Magnetic nanoparticles have been used to determine nodal cancer stage due to their natural deposition into lymph nodes post-injection. Magnetic hyperthermia involves the application of magnetic nanoparticles under the influence of an alternating magnetic field in order to generate elevated temperatures within a target location.

This study aims to investigate the cell killing effect of magnetic hyperthermia in MDA-MB-231 cells in a lymph node *in vitro* model based on its geometric conditions, promising magnetic nanoparticle concentration, and feasible alternating magnetic field parameters. Evaluation was performed with trypan blue exclusion, annexin-V APC / PI flow cytometry and MTT assays.

Acknowledgements

I would like to express my utmost gratitude to my supervisor Dr. Carl Kumaradas in his constant diligence and supervision during my time here at Ryerson. Thank you for being patient with me as I stumbled in this research field with so much to learn. Also, I wish to convey my sincere appreciation in understanding my research interests and allowing me to share my work within this document.

Next, I'd like to thank my supervisory committee members Dr. Michael Kolios and Dr. Jahan Tavakkoli for always surprising me with wise, abstract questions and concepts. In specific to Dr. Raffi Karshafian, I am particularly grateful that you were willing to join and participate in my examination committee despite the short notice.

Now, I would like to extend my gratitude to Elizabeth Berndl for all of the enlightening guidance over the cell culture work, in which I had no prior experience. I would like to acknowledge Arthur Worthington for all of his hard work in drafting and constructing the waterbath container that has been a central and imperative element in my research efforts. Also, I'd like to salute Graham Pearson, Luke Yaraskavitch, and Kevin Liu for the vast array of assistance during numerous late nights of troubleshooting.

Many thanks to George Noble for his bountiful support in my technical questions. I'd like to thank Besiki Surguladze for the supply of the magnetic nanoparticles used in my research and for our intellectual conversations over coffee.

Eric Da Silva and Gabriella Mankovskii, thank you so much for taking the time out of your busy schedules in order to assist me with your wonderful knowledge of total x-ray fluorescence. Much appreciation goes to the other half of JCK Enterprises: Daniel Dicenzo,

thanks for all of my sporadic fact checking and exchanging of ideas. Also to my colleagues Alexandru Nicolae and Humza Nusrat, I cannot believe that it's 'HAP'pening: my time at Ryerson working with you guys on the abundance of coursework and projects is coming to an end and I will definitely miss that. I'd like to also extend a thank you to everyone in the Physics department, as I will never forget the atmosphere of such a warm, welcoming environment as I arrived to Toronto not knowing a single person; I will forever cherish the memories I shared with everyone here.

Furthermore, I would like to thank my family, even if miles away, who always encouraged and believed in the work that I was doing. Finally, Julie, I would not be where I am if it was not for you, so thank you for always pushing me above my limits this past decade.

Quae medicamenta non sanant, ferum sanat.

Quae ferum non sanat, ignis sanat.

Quae vero ignis non sanat, insanobilia reportari oportet.

Those who cannot be cured by medicine can be cured by surgery.

Those who cannot be cured by surgery can be cured by heat.

Those who cannot be cured by heat are to be considered incurable.

Hippocrates, 460 – 370 BC

Table of Contents

List of Tables

List of Figures

Symbols and Abbreviations

AMF – Alternating Magnetic Field

APC – Allophycocyanin

$CEM_{43\,°C}$ – Cumulative Equivalent Minutes at 43 °C

DMEM – Dulbecco's Modified Eagle's Medium

DMSO – Dimethyl Sulfoxide

MDA-MB-231 – Human Breast Adenocarcinoma Cells

MH – Magnetic Hyperthermia

MNP – Magnetic Nanoparticle

MRI – Magnetic Resonance Imaging

PBS – Phosphate Buffer Saline

PI – Propidium Iodide

PS – Phosphatidylserine

SLN – Sentinel Lymph Node

SLNB – Sentinel Lymph Node Biopsy

Chapter 1

Introduction

Nearly half of all Canadians will be diagnosed with cancer during their lifetime; a quarter of that population are expected to die due to this overwhelming disease (Canadian Cancer Society, 2015). The development of cancer is based on the accelerated reproductive nature of mutated cells that leads to the formation of tumors. This condition progresses further with the dissemination of cancer cells throughout the body in a process known as metastasis. Metastasis employs an assortment of routes to circulate through the body such as the bloodstream or the lymphatic system (Nathanson, 2003). Common treatments involve the application of radiation and/or chemotherapeutic drugs targeted over substantial regions of the body in order to eradicate traces of metastasis (Shao, et al., 2013). Prognosis for a patient with metastasis diagnosis becomes a highly complicated assessment as it is difficult to fully eliminate the spread of metastatic cells without severe losses in the quality of life.

1.1 Metastasis in the Lymphatic System

The immune system utilizes the lymphatic system to collect and transport interstitial fluids through lymphatic capillaries to the lymph nodes. Macrophages found in lymph absorb an array of foreign entities, including metastatic cancer cells, to be processed and filtered within the lymph node. The movement of lymph passing through these nodes is unidirectional, meaning that the pathways are limited to a discrete succession of nodes. Eventually, these refined resources are drained back into the bloodstream (Saraf, et al., 2011; Sleeman, et al., 2009).

However, due to the chaotic nature of cancer cells, the collected number of cells may overwhelm the lymph node, forming a secondary tumor, which provides additional access points for metastasis to proceed further into the lymphatic system.

1.1.1 Current Biopsy Techniques

Prognosis is dependent on the ability to detect for the presence and severity in the stage of metastasis. The traditional method involves the complete extraction of the lymph nodes surrounding the primary tumor, which is often referred to as regional lymph node dissection. Following surgical extraction, each lymph node is analyzed for traces of metastatic cells. Depending on the outcome, postoperative treatments such as radiation and/or chemotherapy are prescribed in order to eliminate surviving metastatic cells within that region. Consequently, this procedure requires a mass removal of potentially healthy lymph nodes needed to maintain the function of the immune system. Other complications that can arise from these treatments ranging from the bruising and infections as a result of surgery to the absence of lymph flow management leading to conditions such as lymphedema (Ahmed & Douek, 2013).

Subsequently, the clinical approval of sentinel lymph node biopsy (SLNB) outdates the extensive extraction of the regional lymph nodes by limiting its search to only a select number of nodes based on the sentinel lymph node concept. This concept stems from the understanding that the sentinel lymph node (SLN) is the first one of the lymph nodes to collect lymphatic drainage from a surrounding primary tumor. The term “sentinel” represents the vanguard role of the SLN as it deters additional metastatic cells from continuing further through the network of lymph nodes (Shauer, et al., 2005). After analysis for the presence of metastasis in the SLN, it is safe to

assert that the regional lymph nodes are unaffected if the SLN does not contain metastatic cells. SLNB incorporates the injection of metastable technetium-99 (^{99m}Tc) and/or isosulfan blue dye into the vicinity of the tumor region. The injected fluids will be collected and drained into the SLN, in which the detection of ^{99m}Tc with a handheld gamma probe stipulates the location. The visual staining of the SLN is achieved by the isosulfan blue dye, which provides a clear distinction for which nodes surgically remove (Ahmed & Douek, 2014).

This biopsy tool has not yet been fully implemented in all hospitals due to a few limitations: 1) The handling of radioisotopes in the clinical setting requires appropriate training and disposal protocols; 2) The availability of the rapid decaying ^{99m}Tc parent isotope molybdenum-99, ^{99}Mo, limits the procedure based on the available supply (Ahmed & Douek, 2013; Ahmed & Douek, 2014); and 3) The time it takes for isosulfan blue dye to dissipate out of the system is quick, and therefore should be conducted in a very short amount of time post-injection. This procedure will result in a fewer number of nodes being removed; however, it calls for an invasive surgery at the expense of removing potentially healthy lymph nodes. In order to check for the presence of metastasis, postoperative treatments still must be conducted to eliminate remaining cancer cells.

1.1.2 Metastasis Profiling with Magnetic Nanoparticles

Standard imaging diagnostic tools such as ultrasound, computed tomography, and magnetic resonance imaging serve as suitable approaches to outline the location of lymph nodes. However, the delineation of a lymph node affected by metastasis cannot be verified due to inadequate contrast by using these imaging techniques alone. An alternative to SLNB involves the

utilization of magnetic nanoparticles (MNPs). MNPs have been investigated in several applications such as magnetic targeting for drug and gene delivery, imaging contrast agents, and therapeutic hyperthermia. These applications employ the characteristics of MNPs, which involve its magnetic properties, biocompatibility, and its ability to modify its surface (Pankhurst, et al., 2003; Pankhurst, et al., 2009; Berry & Curtis, 2003; Dutz & Hergt, 2014).

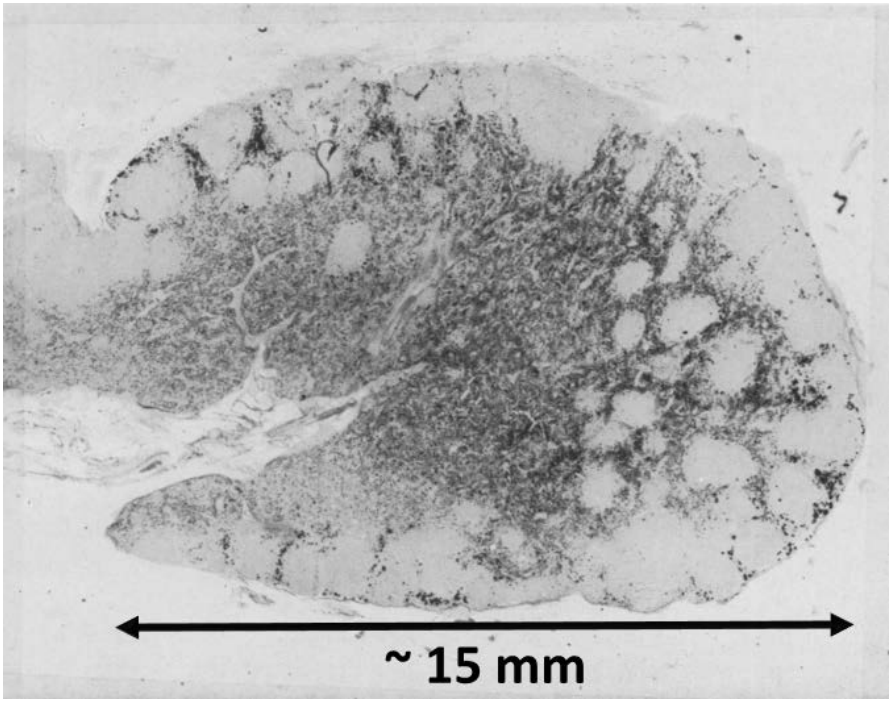

Figure 1: Photomicrograph of a dog specimen demonstrating magnetic nanoparticle deposition in lymph nodes. The distribution of nanoparticles is depicted by the dark regions, which are revealed by the Prussian blue staining of nanoparticles. Adapted figure from (Gilchrist, et al., 1957).

The deposition and movement of MNPs within the lymphatic system have been analyzed in a number of studies. Figure 1 illustrates one of the earliest photomicrographs of MNP deposition of a lymph node (Gilchrist, et al., 1957). Surguladze et al. presented a novel method for detecting SLNs with the use of their prepared MNP fluid (Unimag, Innovative Biomedical

Technologies Inc., Toronto, ON) through interstitial injection. This method was performed on female patients with histologically confirmed instances of breast cancer. The result indicated the retention of Unimag inside the lymph node based on the visual staining on the outside layer of the SLN as seen in Figure 2 (Surguladze, et al., 2011).

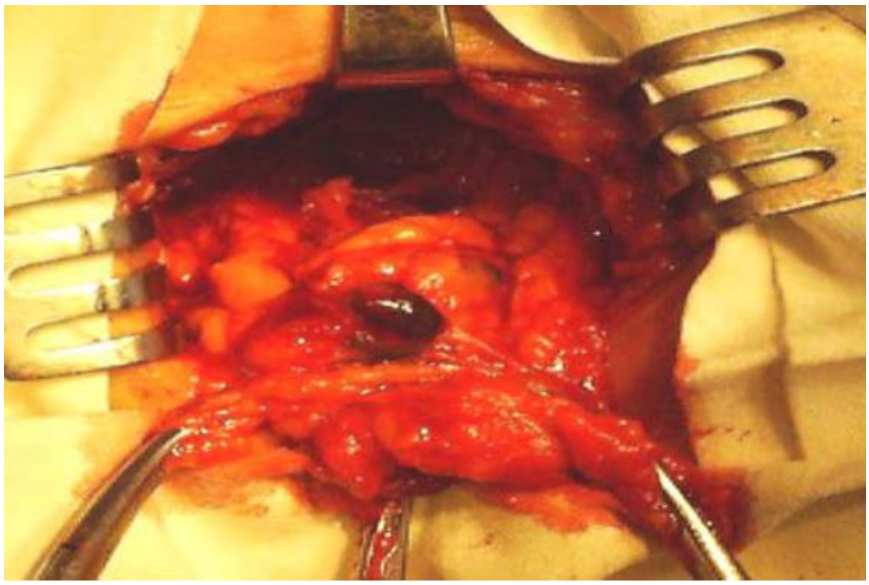

Figure 2: Visual staining of a lymph node after uptake of Unimag magnetic nanoparticles following interstitial injection into a breast cancer patient. Figure obtained from (Surguladze, et al., 2011).

A distribution study of MNP within a lymph node post interstitial injection, based off of an *in vivo* mouse model, was investigated by Finas et al. with clinically available magnetic resonance imaging contrast agent MNP (Resovist, Bayer Schering Pharma AG, Leverkusen, Germany). The observation led to the conclusion that Resovist had accumulated in macrophages that were located inside the lymph node cortex regions (Finas, et al., 2012). These studies propose that MNPs possess the passive capability to become naturally collected and stored inside the SLN through macrophage absorption post-injection.

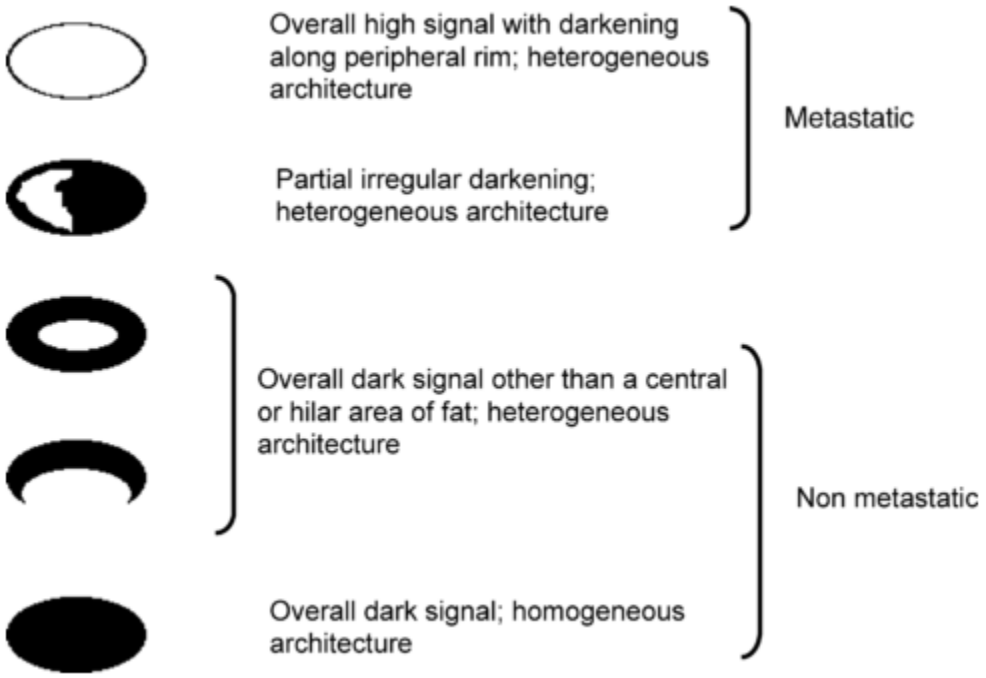

Figure 3: Metastatic diagnostic criteria of superparamagnetic iron oxide nanoparticles in T2*-weighted images. Figure obtained from (Harada, et al., 2007).

Studies have also demonstrated the capabilities of MNP in profiling nodal cancer staging noninvasively with magnetic resonance imaging (MRI). Based on the shifting of signal-to-noise ratio (SNR) in T2*-weighted images, a benign lymph node can be differentiated from a malignant lymph node without the need for surgical dissection (Harisinghani, et al., 2007; Harada, et al., 2007; Johnson, et al., 2010; Johnson, et al., 2013). The prospect in this method of characterization, as outlined in Figure 3, relies on the collection of metastatic cells occupying space within the lymph node, in which circulating MNP will not be able to enter the node causing a constant high MRI signal.

Table 1: Lymph node uptake of indium-labeled monocrystalline iron oxide nanocompounds as converted from percentage of injected dose per gram of tissue. Data collected from (Wunderbaldinger, et al., 2002). [Calculations found in the Appendix, section A.1].

Nodal Cancer Stage	**Concentration (mg Fe/mL)**
Normal Lymph Node	10.9
Micromestastatic	3.19
Small Metastases	1.01
Large Metastases	0.263

This observation further supports the premise proposed by Wunderbaldinger et al. in the iron uptake intravenously post-injected of *in vivo* mice lymph nodes at different nodal cancer stages. Upon the visual inspection of primary tumor growth, lymph nodes were excised for iron concentration determination (Wunderbaldinger, et al., 2002). A summary of the concentrations can be found in Table 1. The efficacy of MNPs in SLN detection and nodal cancer staging have been thoroughly demonstrated; however, the potential of MNPs with its heating capabilities proposes theranostic aptitude in controlling metastasis within the lymphatic system.

1.2 Hyperthermia

As early as 3000 BC, hyperthermia had been sought out as the sole cure for malignant superficial cancers through caustic methods. Hippocrates (460 – 370 BC) had briefly described this notion of heat therapy in his famous aphorism (from Latin translation in Seegenschmiedt & Vernon, 1995):

"Those who cannot be cured by medicine can be cured by surgery.

Those who cannot be cured by surgery can be cured by heat.

Those who cannot be cured by heat are to be considered incurable."

Hyperthermia remains a viable therapy in managing cancer among other treatment modalities such as surgery, radiation therapy, and chemotherapy. Hyperthermia is achieved by elevating temperatures above 40 °C (Van der Zee, 2002). Compared to the DNA strand breakage effects that ionizing radiation has on cells, hyperthermic temperatures denature the cellular membrane and disrupts the transportation functionality of incoming necessary nutrients and proteins that regulate the cell as observed *in vitro* (Okamoto, et al., 1988; Asita & Salehhuddin, 2013; Lee, et al., 2014). These effects often lead to apoptosis, also known as programmed cell death, while higher temperatures (greater than 46 °C) demonstrate charring and burning effects in a matter of seconds, leading to necrosis, or immediate cell death (Hildebrandt, et al., 2002).

Hyperthermia can be applied either as a local, regional, or whole-body prescription depending on the target. Modes of heating are achieved through the utilization of microwaves, radiofrequency applicators, ultrasound, lasers, hot water, or nanoparticles (Chicheł, et al., 2007). Treating cancers with hyperthermia yields several advantages such as the usage of non-ionizing radiation and non-invasive methods to control the growth of cancer. It also exhibits synergistic effects when coupled with radiation therapy, reducing the radiation dose applied to the patient (Seegenschmiedt & Vernon, 1995; Hall & Giaccia, 2012). All cells, including non-malignant cell lines such as Chinese hamster ovary cells found in Figure 4, exposed to hyperthermia will induce cytotoxic effects; however, sensitivity to hyperthermia between normal and malignant tissues is due to the low pO_2 and pH environments from inadequate blood perfusion found in cancerous

tumors (Van der Zee, 2002). A treatment that administers a precise distribution of heat to be within the target region/tumor will most likely spare surrounding healthy tissue.

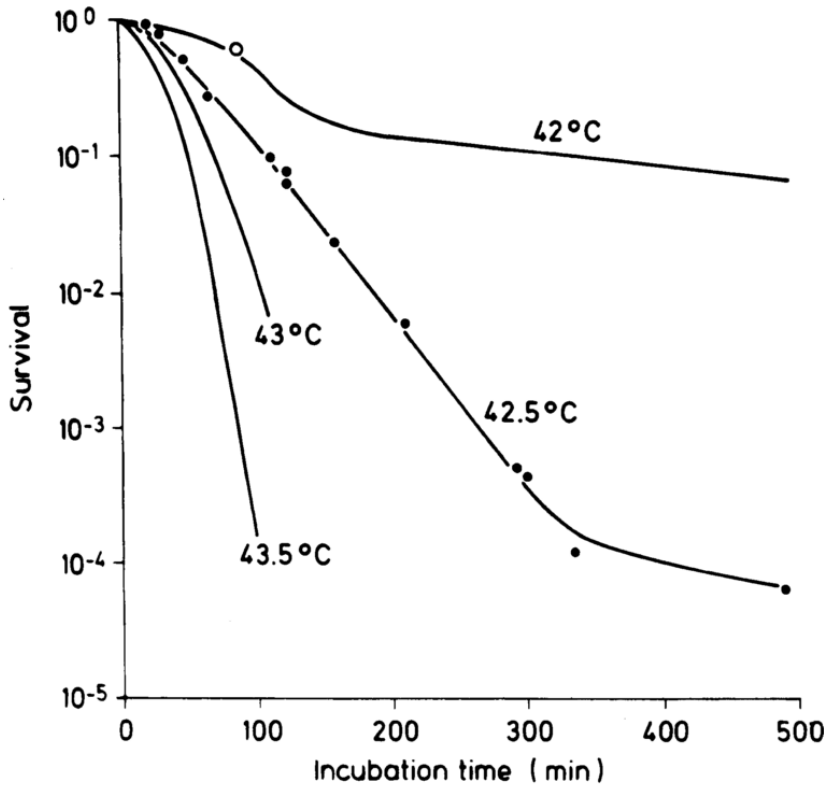

Figure 4: Cell-surviving fraction of Chinese hamster ovary cells under distinct temperatures for varying lengths of time. Figure obtained from (Hildebrandt, et al., 2002).

1.2.1 Thermal Dose

In order to measure the effect of cell killing due to hyperthermia, Sapareto and Dewey established the concept of thermal dose as an exponential relationship between temperature and time. The basis for thermal dose is derived from Dewey's observations on the heating of asynchronous Chinese hamster ovary cells at varying temperatures and periods, where temperatures 43 °C and above portrayed a consistent relationship of the cell survival as found in

Figure 4. However, temperatures below 43 °C demonstrated a decreased rate of cell kill. This thermal effect is measured by the cumulative equivalent minute at 43 °C (CEM_{43}), which is determined by the following relationship:

$$CEM_{43°C} = \sum_{t_i}^{t_f} R^{(43-\bar{T})}\Delta t \quad [1]$$

where $\bar{T}$ represents the average temperature during the time interval Δt, R = 0.50 above 43 °C, and R = 0.25 below 43 °C. This dosimetric parameter emerges as a practical tool in the comparison of the effectiveness between heating at different temperatures and periods (Sapareto & Dewey, 1984; Hall & Giaccia, 2012).

1.3 Magnetic Hyperthermia

Similar to brachytherapy, where the treatment is applied within the target region rather than from exterior surroundings, in magnetic hyperthermia (MH), heat is generated inside the target region to eradicate the presence of cancer. MH uses heat generated by MNPs under the influence of an alternating magnetic field (AMF). MH takes advantage of the nanoparticle and its small size range (< 100 nm) in order to pinpoint the nanoparticle directly inside a specific region/tumor by the enhanced permeability and retention effect for maximum temperature elevation while sparing nearby healthy tissue (Giustini, et al., 2010; Huang & Hainfeld, 2013). Clinical studies have begun demonstrating the efficacy of MH as an adjuvant therapy in patients with glioblastoma multiforme and prostate cancer (Maier-Hauff, et al., 2007; Johannsen, et al., 2007).

1.3.1 Physics of Magnetic Nanoparticle Heating

In addition to the restriction of heating within a target location, properties of the nanoparticle suspension can be controlled in order to govern the rate of heating. Due to their size, MNPs behave superparamagnetically. These superparamagnetic nanoparticles only possess a single magnetic domain, whereas ferromagnetic materials are composed of multiple magnetic domains, each domain pertaining to its own individual magnetic moment (Cardarelli, 2008). As a result, hysteresis losses are negligible in determining the heating capabilities of MNPs, because there exists no magnetic remanence after being exposed to a magnetic field. This superparamagnetic trait contributes significantly to the success of a treatment once injected into the body due to the prevention of agglomeration between the nanoparticles (Laurent, et al., 2011).

MNPs will convert the electromagnetic energy of the AMF into heat energy through relaxational mechanisms when it returns to its equilibrium state. Rotation of the nanoparticle is governed based on its size: whether the magnetic core will rotate through Néel relaxation or the entire particle will spin under Brownian relaxation (Jeyadevan, 2010), as illustrated in Figure 5.

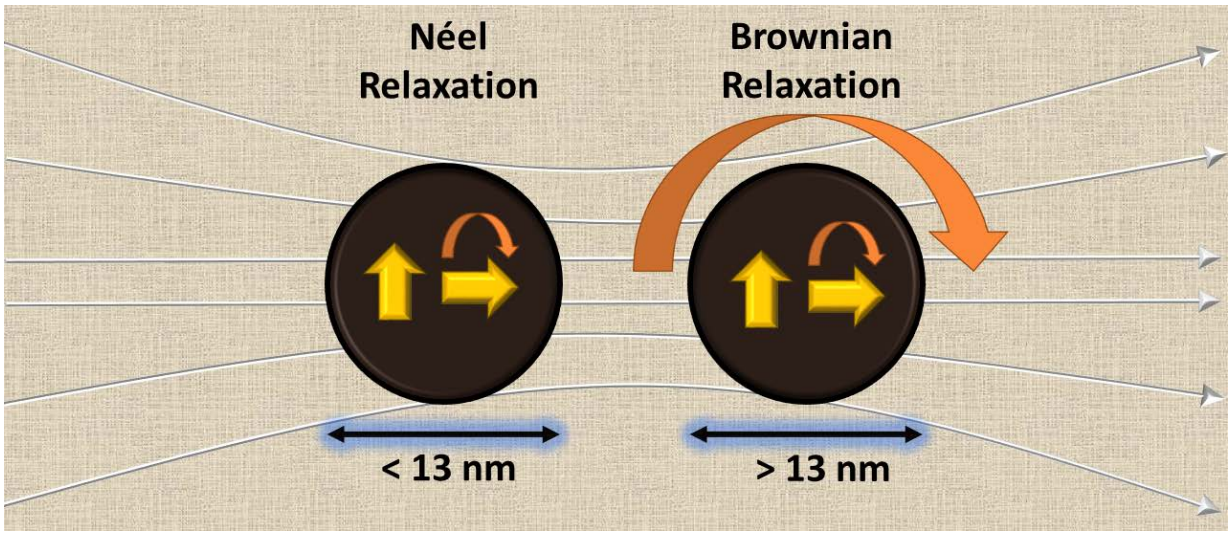

Figure 5: Relaxational mechanisms for magnetic nanoparticles under the influence of an alternating magnetic field: Néel relaxation results in heat generation due to magnetic moment rotation and Brownian relaxation results in heat generation due to the forced rotation of the particle in a viscous fluid. Adapted from (Jeyadevan, 2010).

Particles of less than 13 nm will undergo Néel relaxation, in which the magnetic core of the particle will align with a surrounding magnetic field, leaving the physical particle orientation unchanged. Heat becomes dissipated due to resistance in the magnetic moment's return to equilibrium in phase with the AMF. In contrast, MNPs undergoing Brownian relaxation cause the whole particle, as well as the magnetic moment, to rotate and align with the magnetic field. Due to forced rotation of the particle inside a liquid, friction generates heat as the particle continuously oscillates rotationally under the influence of an AMF. Based on the wide distribution of nanoparticle sizes in a suspension, heat dissipation is calculated based on an average of both relaxation mechanisms (Hergt, et al., 1998; Rosensweig, 2002; Jeyadevan, 2010).

1.3.2 Biophysical Limits on the Alternating Magnetic Field

A challenge in MH is the application of AMFs onto human patients. Non-magnetic material such as healthy tissue will heat due to the production of eddy currents. Based on clinical results, it was recommended that for a heating treatment of one hour with minimal discomfort towards the patient, the product of the AMF strength and its frequency be limited to a threshold, known as the critical product, given by:

$$C = Hf > 5 \times 10^9 \frac{\mathrm{A}}{\mathrm{ms}} \quad [2]$$

where H represents the AMF strength and f represents the frequency of the AMF (Hergt & Dutz, 2007).

1.3.3 Lymph Node Heating

Besides the abundant number of recent studies evaluating the potential of MH, this phenomenon was first demonstrated by Gilchrist et al. in 1957. The objective of their study was to explore the feasibility in MNP heating of the lymph node in order to eliminate missed metastases after initial dissection. After subserosa, subcutaneous, and subperitoneal injections, the group measured for the concentration of MNPs (20 nm – 100 nm) deposited in excised lymph nodes from numerous dogs. The distribution of MNP concentrations inside the lymph nodes is presented in Figure 6.

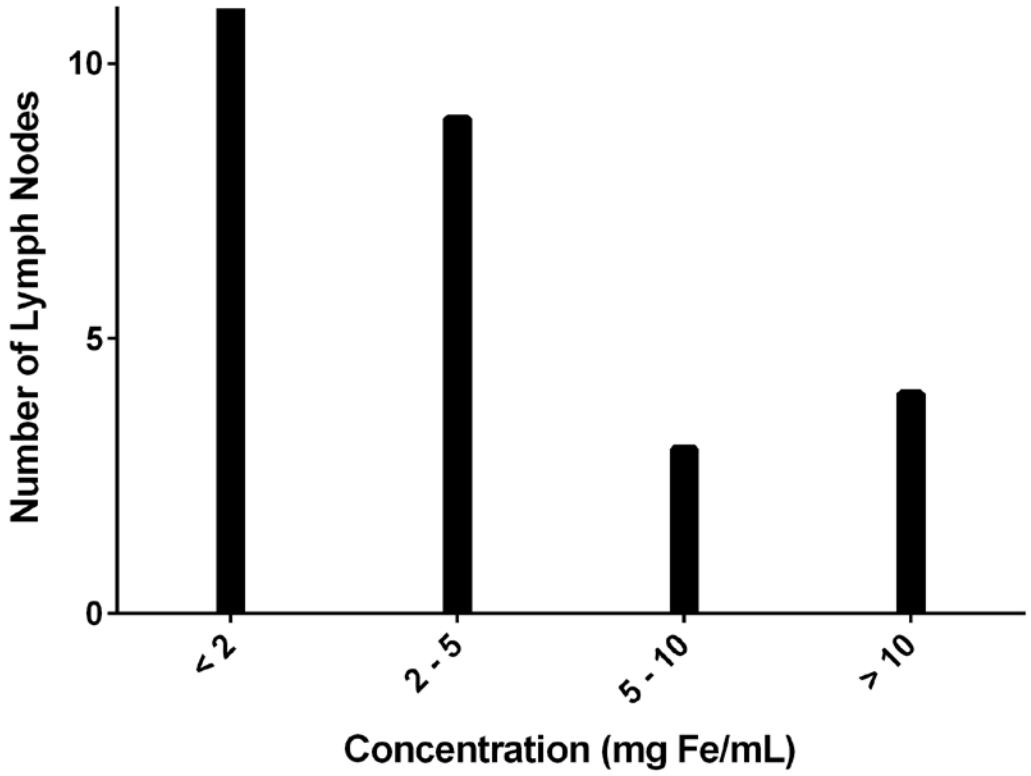

Figure 6: Lymph node uptake of maghemite (Fe_2O_3) magnetic nanoparticles from a single dog specimen after subserosa, subcutaneous, and subperitoneal injections. Data collected from (Gilchrist, et al., 1957).

Heating of the lymph node ex vivo was also demonstrated in this study. An iron concentration of 5 mg Fe/mL was reported for a single excised lymph node, in which AMF strengths between 15.4 and 19.1 kA/m at a frequency of 1200 kHz exhibited a rise of 14 °C within three minutes (Gilchrist, et al., 1957). However, these experiments were conducted during a period where there was little understanding of the parameters involved in MNP heating. For example, the selected AMF strength and frequency clearly exceeds the critical product for a one hour treatment for human patients, which may have resulted in the large rise in temperature due contributions of eddy current heating in surrounding tissue. As seen from the study performed by

Wunderbaldinger et al., it is also important to take into account the nodal cancer stage in order to evaluate the degree of MNP deposition (Wunderbaldinger, et al., 2002).

To the best of my knowledge, a study involving the heating of lymph nodes to control the metastasis in the lymphatic system has not been explored since this report from almost 60 years ago. By utilizing the natural deposition of MNPs in the lymph nodes, MH is an appealing prospect in controlling metastasis in the lymphatic system. This study aims to bring light back into this topic.

1.4 Objective & Specific Aims

The objective of this study was to evaluate the application of MH *in vitro* emulating lymph node *in vivo* conditions.

The specific aims were to 1) simulate a lymph node *in vitro* based on a typical lymph node geometry, a suitable deposited MNP concentration, and AMF at the biophysical limit; 2) determine the temperature that can be obtained in the *in vitro* lymph node model under these conditions; and 3) assess the viability of MDA-MB-231 breast cancer cells in suspensions after a one hour of treatment.

Chapter 2

Materials and Methods

Four conditions were investigated: a control cell suspension with no MNPs, a cell suspension that was heated with a waterbath, a control cell suspension with MNPs and no AMF, and a cell suspension with MNPs and heating via AMF. Three cell viability assays were performed, each measuring a different cell characteristic that affect viability: trypan blue exclusion, annexin-V/PI (flow cytometry), and MTT.

2.1 The Magnetic Nanoparticles

MNP suspension Unimag was supplied through a research collaboration between Innovative Biomedical Technologies, Inc. (Toronto, ON) and Ryerson University. The elemental compound for Unimag is magnetite (Fe_3O_4). The particle surface coatings were comprised of oleic acid, citric acid, soy lecithin, and polysorbate-80 (Surguladze, 2010). The size range of the presented nanoparticles were within 8 – 16 nm (Noble, 2012), as shown in Figure 7. Using transmission electron microscopy analysis, the average diameter was determined to be around 9.18 ± 2.34 nm (Noble, 2012). The concentration of iron in the suspension was measured using total x-ray fluorescence spectroscopy through the S2 PICOFOX (Bruker, Billerica, MA) and was determined to be 69.5 mg Fe/mL.

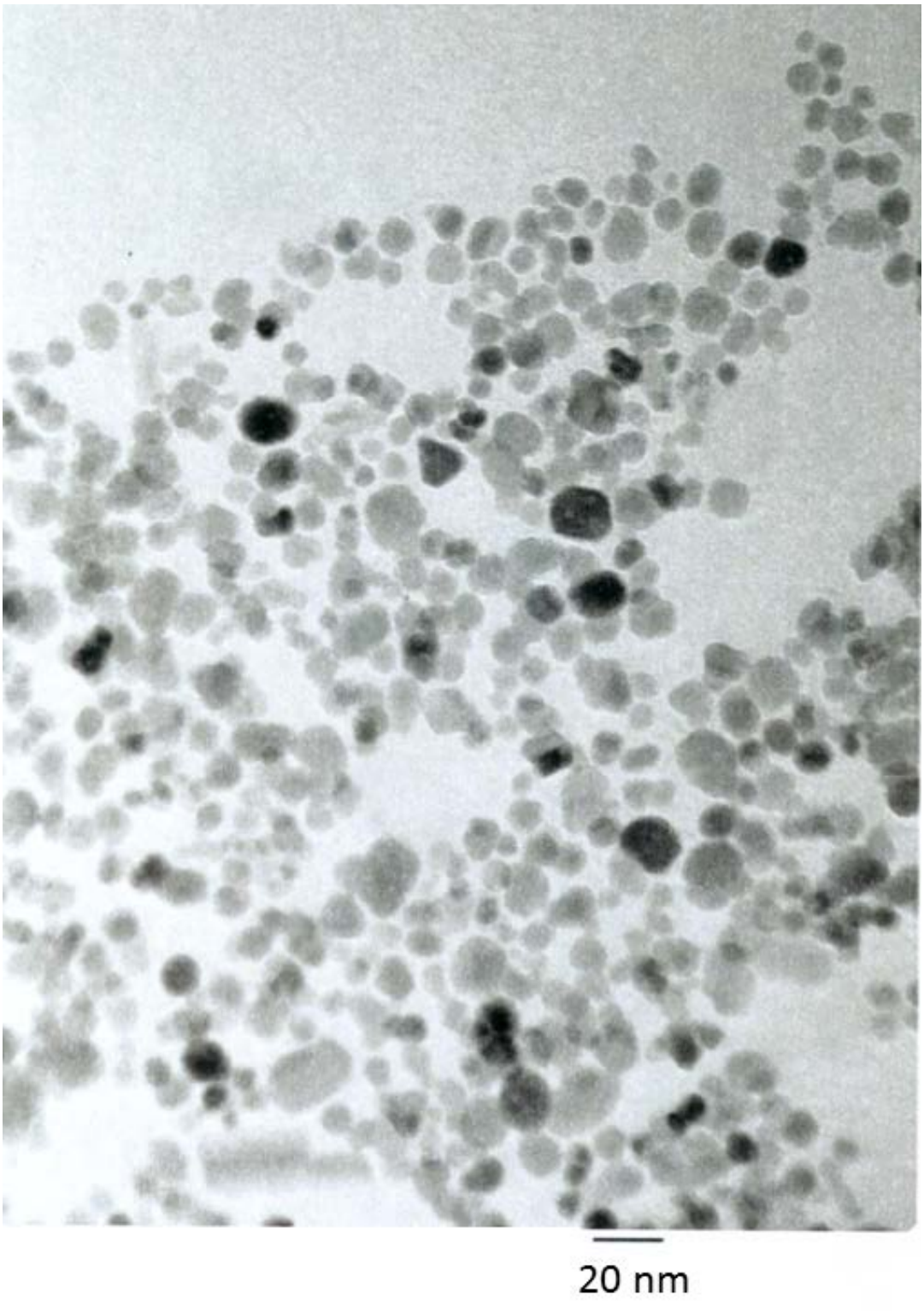

Figure 7: Transmission electron microscopy image of Unimag suspension diluted by volume 1:1000. Adapted figure obtained from (Noble, 2012).

2.2 Magnetic Hyperthermia Apparatus

Figure 8 shows the components used for the experiments and Figure 9 shows the functional relationship between the instruments. AMFs were produced by a 5 kW induction power supply (UltraHeat UPT-W8, Ultraflex Power Technologies, New York, NY) and an external heat station (Model No. ACC-722-100-A00, Ultraflex Power Technologies, New York, NY), which contains a two-turn induction coil with an inner diameter of 4.8 cm. Temperature moderation of the induction system was maintained by water cooling (R2200V Fan, Dynaflux, Cartersville, GA).

AMF parameters (12.3 kA/m and 394 kHz) were chosen based on the critical product, as expressed in Equation 2. As a control for the cell killing due to hyperthermia without the use of MNPs, an additional waterbath (GP-100, Neslab, Newington, NH) set at 44 °C was used to heat the cells. Temperature monitoring was performed by three separate fluoroptic temperature probes (Luxtron Corporation, Santa Clara, CA), which were digitized through a fluoroptic thermometer (3100 Series Fluoroptic Thermometer, Luxtron Corporation, Santa Clara, CA). The temperature measurements from the three probes were averaged to produce a single heating profile and account for inhomogeneous heating distribution due to non-uniform field strengths and natural convection losses (Huang, et al., 2012). The temperature profile was processed and analyzed using the analytical software MATLAB (Version R2015a, Mathworks, Natick, MA).

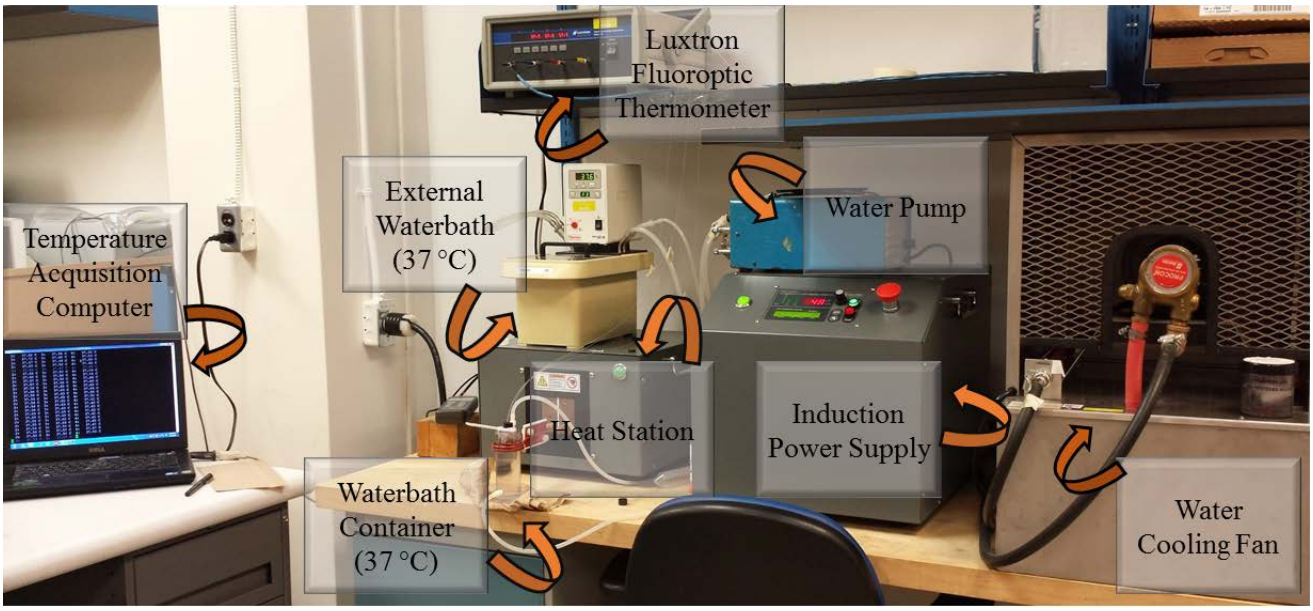

Figure 8: Photograph containing the implemented components in the magnetic hyperthermia apparatus.

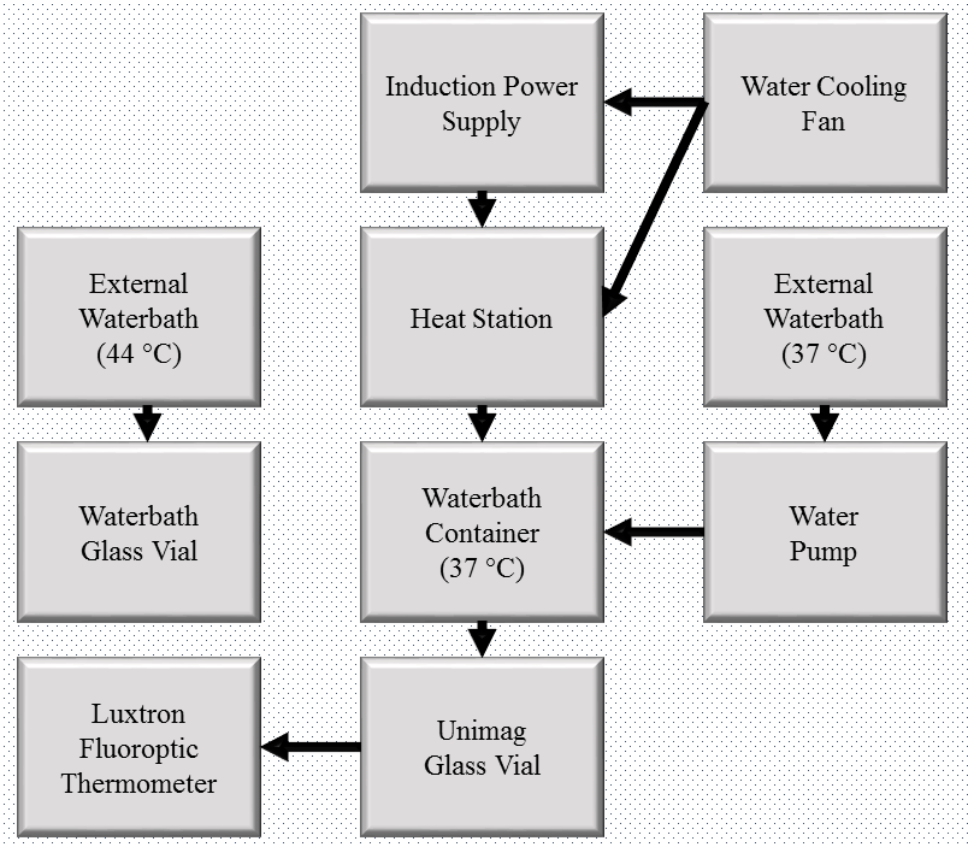

Figure 9: Schematic illustrating the instruments used to accomplish magnetic and conventional hyperthermia.

2.2.1 Replicating *in vivo* Lymph Node Conditions *in vitro*

The size of cancerous human lymph nodes range from 1 mm to 25 mm, depending on the nodal cancer stage (Martini, et al., 2015). In order to best replicate these geometric conditions, a glass vial (Sigma-Aldrich, St. Louis, MO) with an inner diameter of 14 mm was chosen as the cell suspension vessel for the heating experiments. A total volume of 1 mL was selected in order to encompass a height of 7.5 mm, which further mimics the oval-like structure of the lymph node. Surrounding temperatures of 37 °C around the vial was established within a custom-built container, which is illustrated in Figure 10. The temperature was maintained using an external waterbath (Haake P5, Thermo Electron Corporation, Waltham, MA) and peristaltic pump (Model No. 7520-00, Cole-Parmer Instrument Co., Montreal, QC). The waterbath container was positioned in the center of the 48 mm diameter induction coil that was fitted onto the heat station.

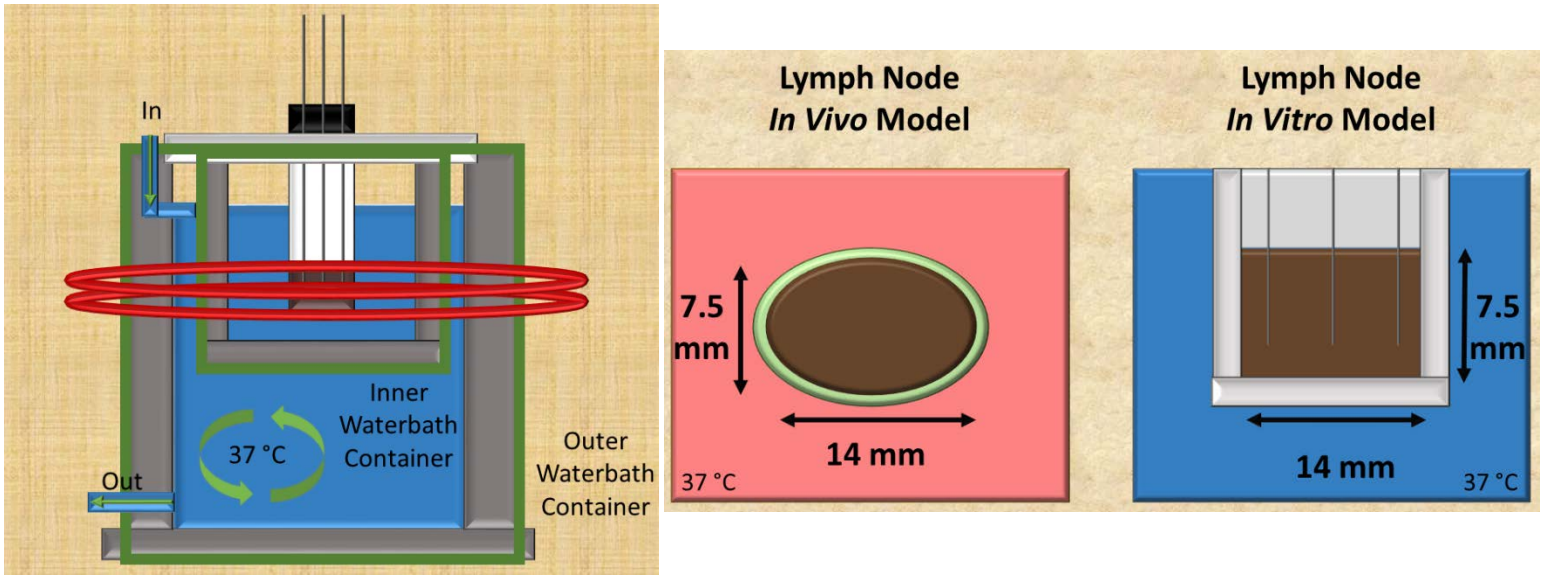

Figure 10: Left – Illustration of the constructed waterbath container and flow of 37 °C water around the glass vial containing cell suspension and Unimag; Right – Comparison of lymph node geometric parameters and surrounding temperature with selected glass vial containing 1 mL cell suspension and Unimag located inside the waterbath container.

The waterbath container is comprised of two components: the outer and inner containers. The outer container utilizes the flow of 37 °C from the external waterbath, whereas the inner container holds non-flowing water, but remains heated from the surrounding outer container. This allows for thermal equilibrium to 37 °C within the inner container, but the flowing water will not interfere with the heat transfer between the glass vial and inner container. This representation provides an accurate depiction for the lack of blood flow within the lymph nodes.

2.3 Cell Culture Studies

The MDA-MB-231 cell line (Human breast adenocarcinoma, ATCC, Manassas, VA) was chosen for the lymph node *in vitro* model. The mammary glands in the breast region plays an integral role in disseminating breast cancer cells through the lymphatic system due to its extensive extravascular drainage. MDA-MB-231 cells exhibit cancer stem cell-like characteristics such as self-renewal and differentiated cell populations, thus being responsible for developing or supplying the tumor environment (Pathak, et al., 2006; Sadhukha, et al., 2013).This cell line is a suitable model of metastatic cells that would be accumulated in lymph nodes.

The cells were cultured in Dulbecco's modified Eagle's medium (DMEM) (Thermo Fisher Scientific, Inc., Waltham, MA) supplemented with 10% fetal bovine serum (Thermo Fisher Scientific, Inc., Waltham, MA) and 1% penicillin streptomycin (Thermo Fisher Scientific, Inc., Waltham, MA). These cells were incubated in 5% carbon dioxide at 37 °C and passaged every four to five days.

2.3.1 Cell Suspension Preparation and Hyperthermia Treatment

At around 90% confluency, the cells were washed with phosphate buffer saline (PBS) (Thermo Fisher Scientific, Inc., Waltham, MA) and then harvested by trypsinization. The number of live cells was then determined by trypan blue dye exclusion through a hemocytometer and an inverted optical microscope. The cells were then centrifuged and resuspended at 3,000,000 cells/mL.

For the control and waterbath conditions, 500 uL of DMEM was added into the 4 mL glass vials, whereas for the Unimag conditions, 457 uL of DMEM and 43 uL of Unimag were added into the 4 mL glass vials in order to obtain the target 3.0 mg Fe/mL concentration. Finally, 500 uL from the resuspended volume was then transferred into respective glass vials for a final volume of 1 mL each at 1,500,000 cells/mL.

The Unimag and MDA-MB-231 preparation was then positioned inside the waterbath container in order to equilibrate to 37 °C prior to one hour of MH treatment at 12.3 kA/m and 394 kHz. The Luxtron probes were sterilized with ethanol alcohol and inserted into the glass vial for temperature monitoring (see Figure 10), prior to applying the AMFs. Concurrent to the MH treatment, a waterbath preparation was heated via a separate waterbath set at 44 °C. During the heating experiments, the control and control Unimag suspensions remain incubated in 5% carbon dioxide at 37 °C. After one hour of heating, each suspension is washed twice with PBS and then resuspended in 3 mL of fresh DMEM in preparation for the cell viability assays.

2.3.2 Immediate Cell Membrane Permeability (Trypan Blue Exclusion)

Cell membrane permeability is generally associated with signs of necrosis due to excessive damage and deterioration. Trypan blue exclusion exploits the passive permeation of trypan blue dye through impaired plasma cell membrane. Intact live cells will actively exclude the dye, in which allows for the differentiation between live and dead cells under a microscope (Strober, 1997). With a 1:1 dilution of MDA-MB-231 cell suspension and 0.4% trypan blue dye solution, the live and dead cells were counted with a hemocytometer. The cell viability, V, was defined as:

$$V = \frac{L}{L+D} \quad [3]$$

where L represents the live cell count and D represents the dead cell count. Live cells were visualized under a microscope as round white spheres and dead cells as blue-stained spheres, which were counted with a hand-counter. Normalized cell viability for treated conditions were determined by dividing treated cell viability by the control cell viability.

2.3.3 Cell Membrane Integrity (Annexin-V APC / PI)

The binding of annexin-V and uptake of propidium iodide (PI) identifies either early or late apoptotic markers expressed by individual cells based on contrasting fluorescent wavelength emissions. Phosphatidylserine (PS) underneath the inner membrane lining flips onto the outer surface, which indicates a cell that has initiated the process of apoptosis. Under proper conditions comprising of sodium chloride and calcium chloride, annexin-V will attach onto cells exposing PS indicating early apoptosis (AV+/PI-). PI enters the cell, and plays a role similar to that of the trypan blue dye. It measures the integrity of the plasma membrane of the cell. Cells with only PI

markers are labeled as necrotic (AV-/PI+); however, cells with both markers are recognized to be at its late apoptotic stage (AV+/PI+). If no markers are present, the analyzed cell is considered to be healthy (AV-/PI-) (Muppidi, et al., 2004). The cell viability, V, was defined as:

$$V = \frac{H}{H+E+L+N} \quad [4]$$

where H represents the healthy cell percentage, E represents the early apoptotic percentage, L represents the late apoptotic percentage, and N represents the necrotic percentage. Normalized cell viability for treated conditions were determined by dividing treated cell viability by the control cell viability.

Following the protocol provided by the annexin-V allophycocyanin (APC) / PI apoptosis detection kit (eBioscience, San Diego, CA), preparation for flow cytometry measurements included additional wash phases each with PBS and 1x binding buffer. Cells were then resuspended to 2,500,000 cells/mL with 1x binding buffer. 100 uL was transferred into a 5 mL round-bottom tube (Corning, Inc., Corning, NY) and 5 uL of annexin-V APC conjugate was added. After 15 minutes of incubation at room temperature in the dark, 5 uL of PI was added. Tubes were then processed through the BD LSRFortressa X-20 flow cytometer and analyzed using the BD FACSDiva 8.0.1 software (BD Biosciences, San Jose, CA).

2.3.4 Proliferative/Metabolic Ability (MTT Assay)

The reduction of yellow tetrazolium salt, MTT (3-(4, 5-dimethylthiazolyl-2)-2, 5-diphenyltetrazolium bromide), into an insoluble purple formazan by metabolically active cells demonstrates the proliferative capabilities of the cells. Following the introduction of a

solubilization solution such as dimethyl sulfoxide (DMSO) leading to the rupture of the formazan-containing cells, the light intensity of the suspension can be analyzed with a spectrophotometer. Decreased intensities indicate the decline in proliferative ability of the cells illustrating its inoperative function, which is recognized as cell death (Riss, et al., 2004). The normalized cell viability, V_N, was defined as:

$$V_N = \frac{I}{I_C} \quad [5]$$

where I represents the intensity of the metabolized MTT (purple color) from the applied treatment and I_C represents the intensity of the metabolized MTT (purple color) from the control.

For each condition the each cell suspension was resuspended to 100,000 cells/mL. An added condition of control Unimag was prepared in order to account for background subtraction due to the presence of the Unimag nanoparticles. Twelve aliquots of 100 uL for each condition were then transferred to a row of a 96 well plate (Sarstedt AG & Co., Nümbrecht, Germany). Following 24 hours of incubation in 5% carbon dioxide at 37 °C, each well was carefully aspirated. 100 uL of .084% MTT (Sigma-Aldrich, St. Louis, MO) and DMEM mixture was then added to each condition row except the Unimag background control, where only DMEM without MTT was added. The well plate was incubated further in 5% carbon dioxide at 37 °C for two hours. Liquid from the wells were again aspirated, and 100 uL of DMSO was added to each well. After ten minutes of incubation at room temperature in the dark, the well plate was to be read by the colorimetric plate reader SpectraMax M5e and analyzed with SoftMax Pro software (Molecular Devices, LLC, Sunnyvale, CA).

Chapter 3

Results

Cell viability studies were evaluated and plotted with analysis software Prism 6 (GraphPad Software, Inc., La Jolla, CA). A total of four trials were sampled and used for analysis. Four conditions were explored in this study.

3.1 Heating Temperature Profile

In order to verify that the inner waterbath container (Figure 10) was maintaining a steady temperature of 37 °C surrounding the glass vial, two sets of measurements (one with the AMF on and the other with the AMF off) with 1 mL of milli-Q water were performed. They are shown in Figure 11. Over the course of two hours, the mean temperature, with the AMF present, was calculated as 37.24 ± 0.10 °C, whereas with the 5 kW induction power supply turned off, the mean temperature was calculated as 37.02 ± 0.09 °C. The difference due to the presence of AMFs for milli-Q water inside the waterbath container was determined to be 0.22 ± 0.13 °C.

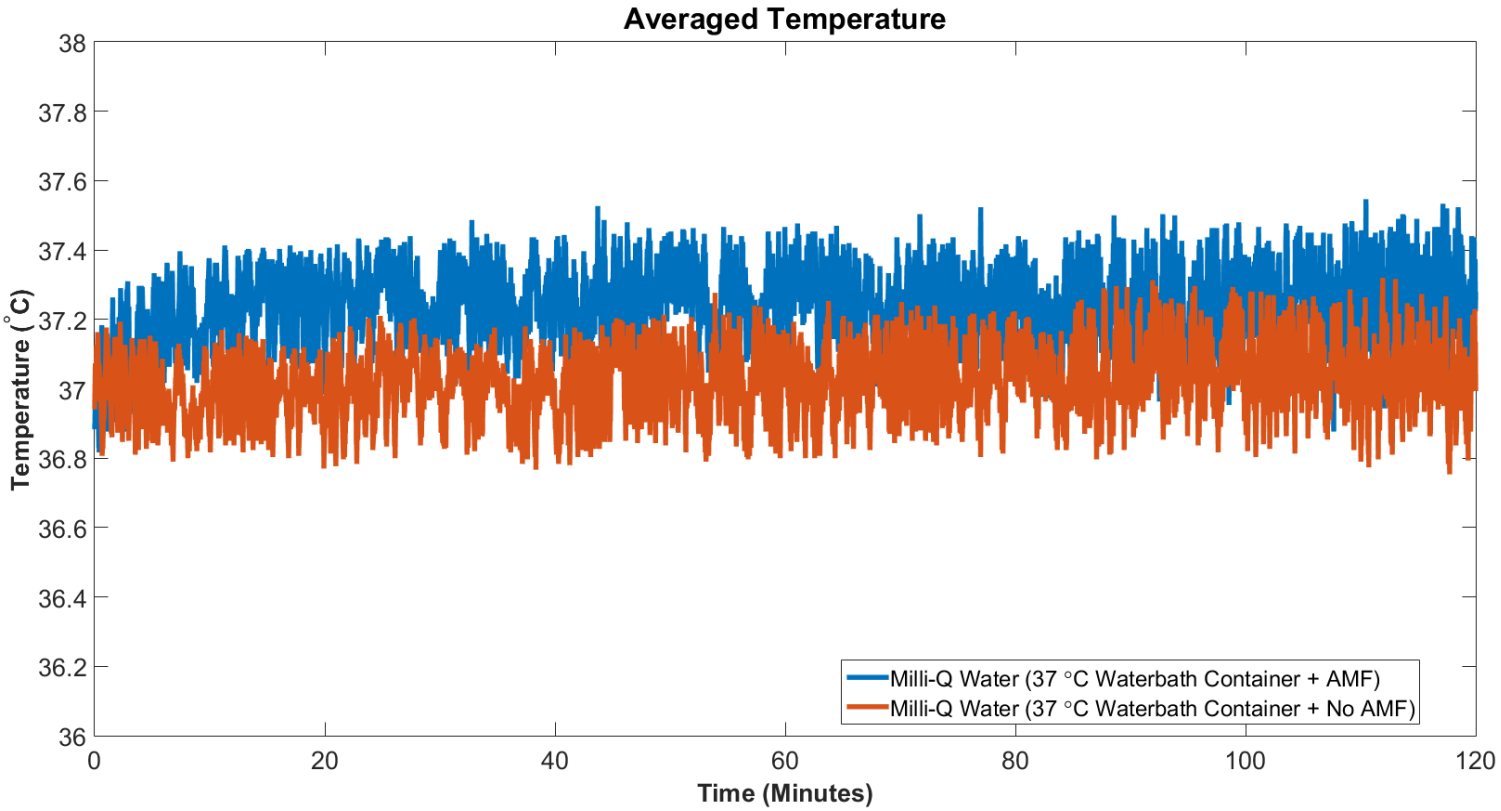

Figure 11: Two hour temperature measurement of milli-Q water (1 mL) inside waterbath container under two conditions: blue) alternating magnetic field (12.3 kA/m and 394 kHz) turned on; red) no alternating magnetic field.

Four sets of trials were observed and respective temperatures were averaged during the course of a one hour MH measurement for 3.0 mg Fe/mL cell suspensions. The average starting temperature was 36.51 ± 0.07 °C. The average times to reach 43 and 44 °C were 1.87 ± 0.25 and 7.34 ± 2.08 minutes, respectively. A temperature of 44 °C was achieved; however, throughout the heating experiment, the temperature of the cell suspension would drop to an average temperature of 43.72 ± 0.60 °C. Individual $CEM_{43\ °C}$ values were calculated using Equation 1 and are displayed in the legend of Figure 12; the average $CEM_{43\ °C}$ was 100.75 ± 0.96 minutes.

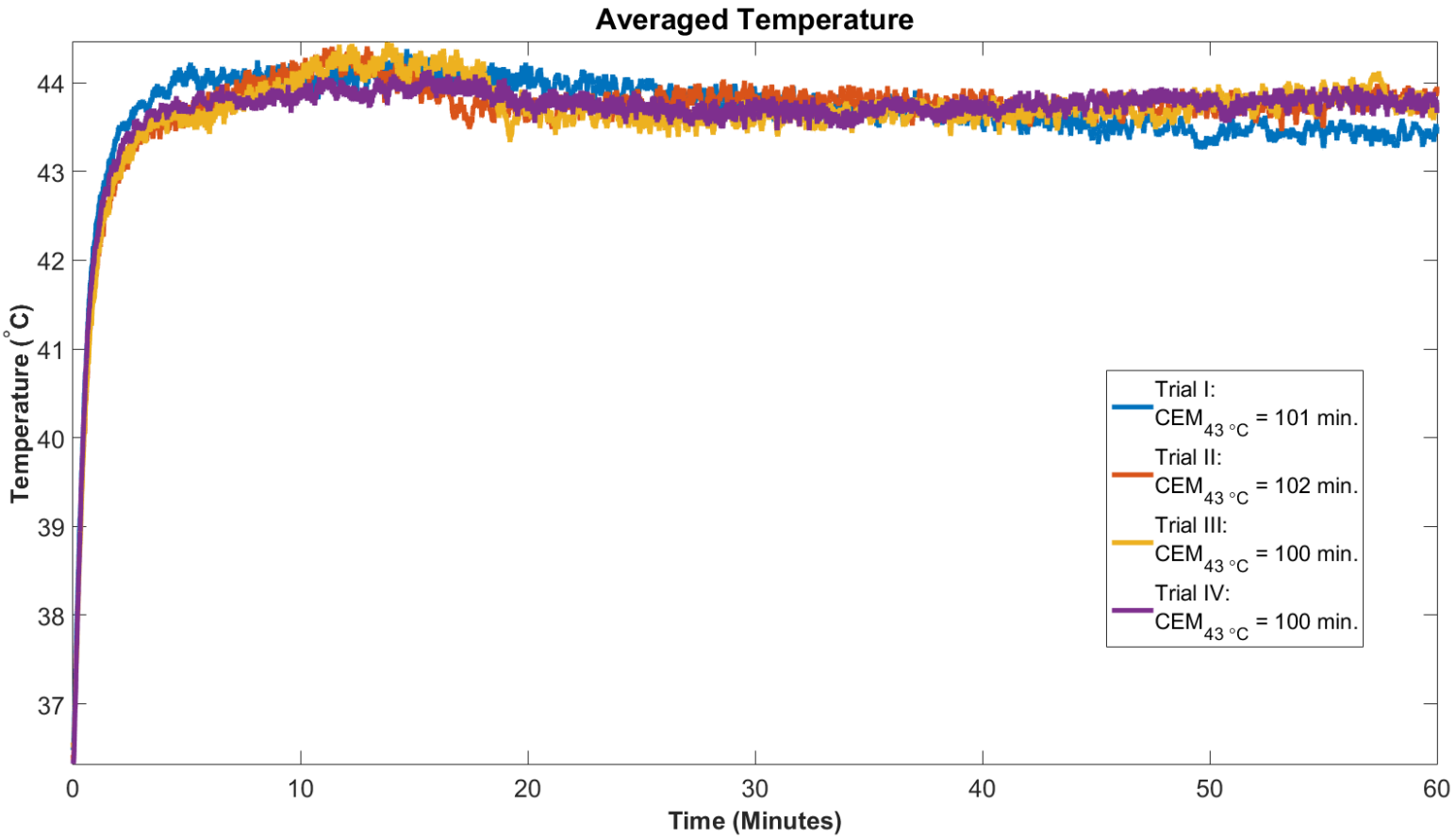

Figure 12: Magnetic hyperthermia temperature profile of trials I – IV for MDA-MB-231 and Unimag (3.0 mg Fe/mL) cell suspension after one hour heating in the waterbath container and alternating magnetic field presence (12.3 kA/m and 394 kHz).

3.2 Cell Viability

Three viability assays were explored in order to assess cell membrane permeability and integrity and cellular metabolic functionality. Normalized viability percentages were calculated based on treated cell viability divided by the control cell viability. Statistical analysis was evaluated under an unpaired t-test where $p < 0.05$ were considered statistically significant.

3.2.1 Immediate Cell Membrane Permeability (Trypan Blue Exclusion)

Cell viability, as defined in Equation 3, was assessed through the immediate cell membrane permeability using the trypan blue exclusion protocol. The results are shown in Figure 13. MDA-MB-231 cells in the presence of Unimag without heat exhibited 91.04 ± 4.37% cell viability, however, when induced with MH, cell viability dropped to 50.93 ± 9.55% ($p < 0.001$). In comparison, conventional hyperthermia with an external waterbath presented a cell viability of 95.42 ± 1.72% ($p < 0.0001$).

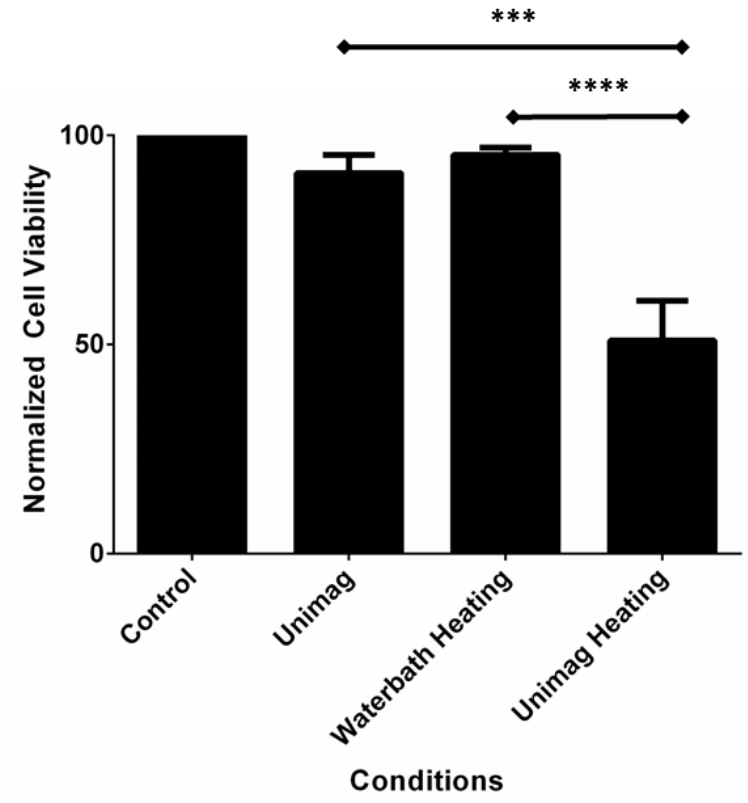

Figure 13: Immediate cell membrane permeability assessed using the trypan blue exclusion protocol one hour after the presence of magnetic nanoparticles, conventional hyperthermia, or magnetic hyperthermia. Respectively, normalized cell viability values are 91.04 ± 4.37%, 95.42 ± 1.72%, and 50.93 ± 9.55%. Data is represented as mean ± standard deviation for $n = 4$; *** and **** represents $p < 0.001$ and $p < 0.0001$, respectively.

3.2.2 Cell Membrane Integrity (Annexin-V APC / PI)

Cell membrane integrity was determined by flow cytometry under the annexin-V / PI protocol indicating evidence for early/late apoptotic and necrotic deaths. These results can be found in Figure 14. MDA-MB-231 cells in the presence of Unimag without heat exhibited 71.89 ± 15.95% cell viability, however, when induced with MH, cell viability dropped to 43.62 ± 3.15% ($p < 0.05$). In comparison, conventional hyperthermia with an external waterbath presented a cell viability of 102.61 ± 5.37% ($p < 0.0001$).

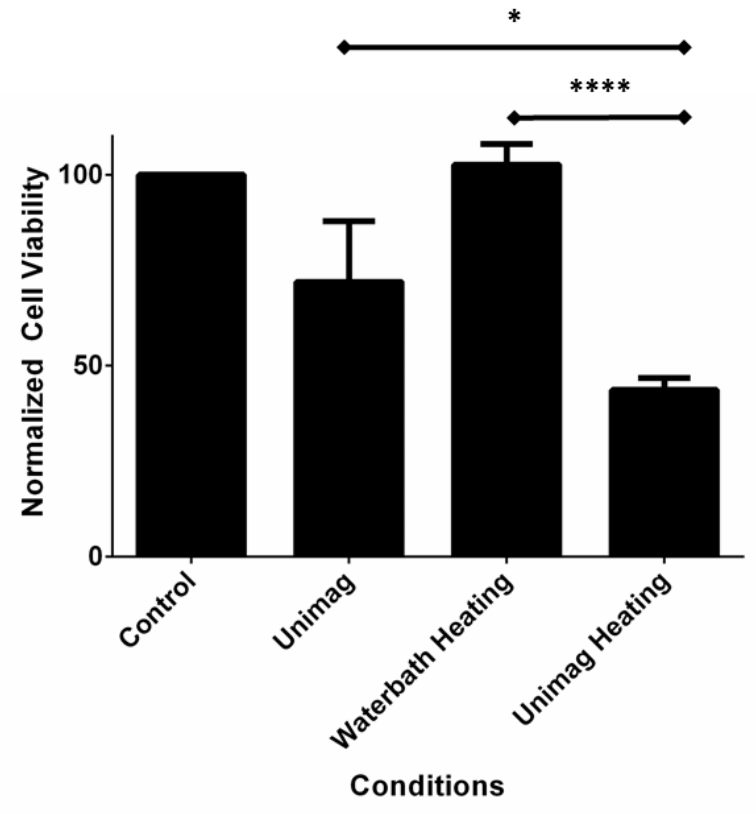

Figure 14: Cell membrane integrity assessed using annexin-V APC / PI protocol after one hour of presence of magnetic nanoparticles, conventional hyperthermia, or magnetic hyperthermia. Respectively, normalized cell viability values are 71.89 ± 15.95%, 102.61 ± 5.37%, and 43.62 ± 3.15%. Data is represented as mean ± standard deviation for $n = 4$; * and **** represents $p < 0.05$ and $p < 0.0001$, respectively. Supplementary flow cytometry averaged results can be found under the Appendix section 6.2.

3.2.3 Proliferative/Metabolic Ability (MTT Assay)

Proliferative and metabolic activity was evaluated by colorimetry based on the ingestion of MTT salt indicating the survival and growth of cells 24 hours after treatment. These results are shown in Figure 15. MDA-MB-231 cells in the presence of Unimag without heat exhibited 62.72 ± 15.12% cell viability, however, when induced with MH, cell viability dropped to 15.47 ± 11.04% ($p < 0.01$). In comparison, conventional hyperthermia with an external waterbath presented a cell viability of 50.07 ± 10.54% ($p < 0.01$).

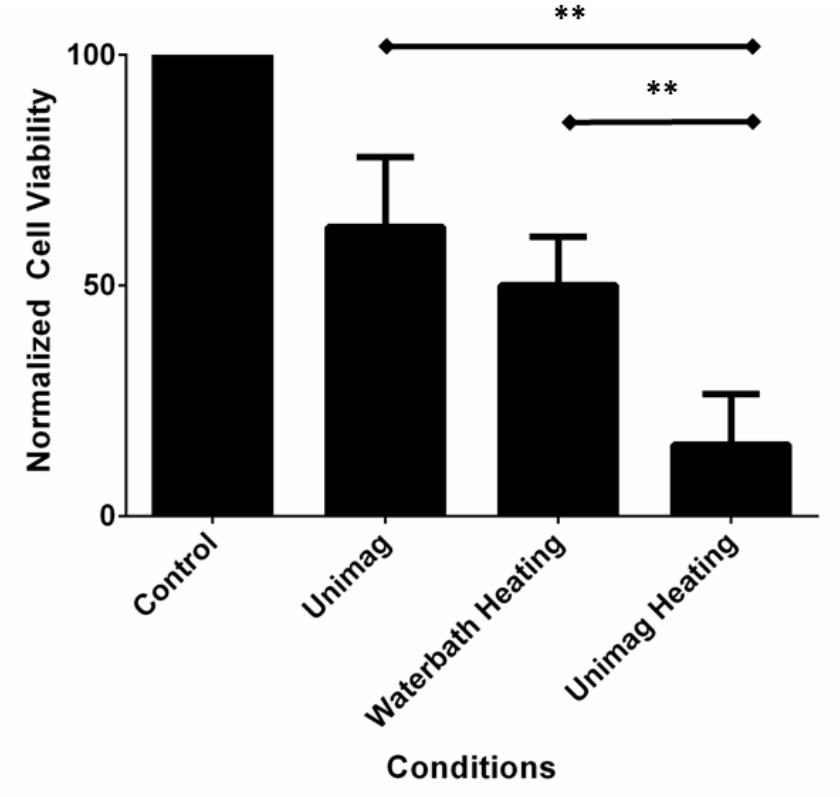

Figure 15: Proliferative and metabolic ability assessed by MTT assay after one hour of presence of magnetic nanoparticles, conventional hyperthermia, or magnetic hyperthermia. Respectively, normalized cell viability values are 62.72 ± 15.12%, 50.07 ± 10.54%, and 15.47 ± 11.04%. Data is represented as mean ± standard deviation for $n = 4$; ** represents $p < 0.01$.

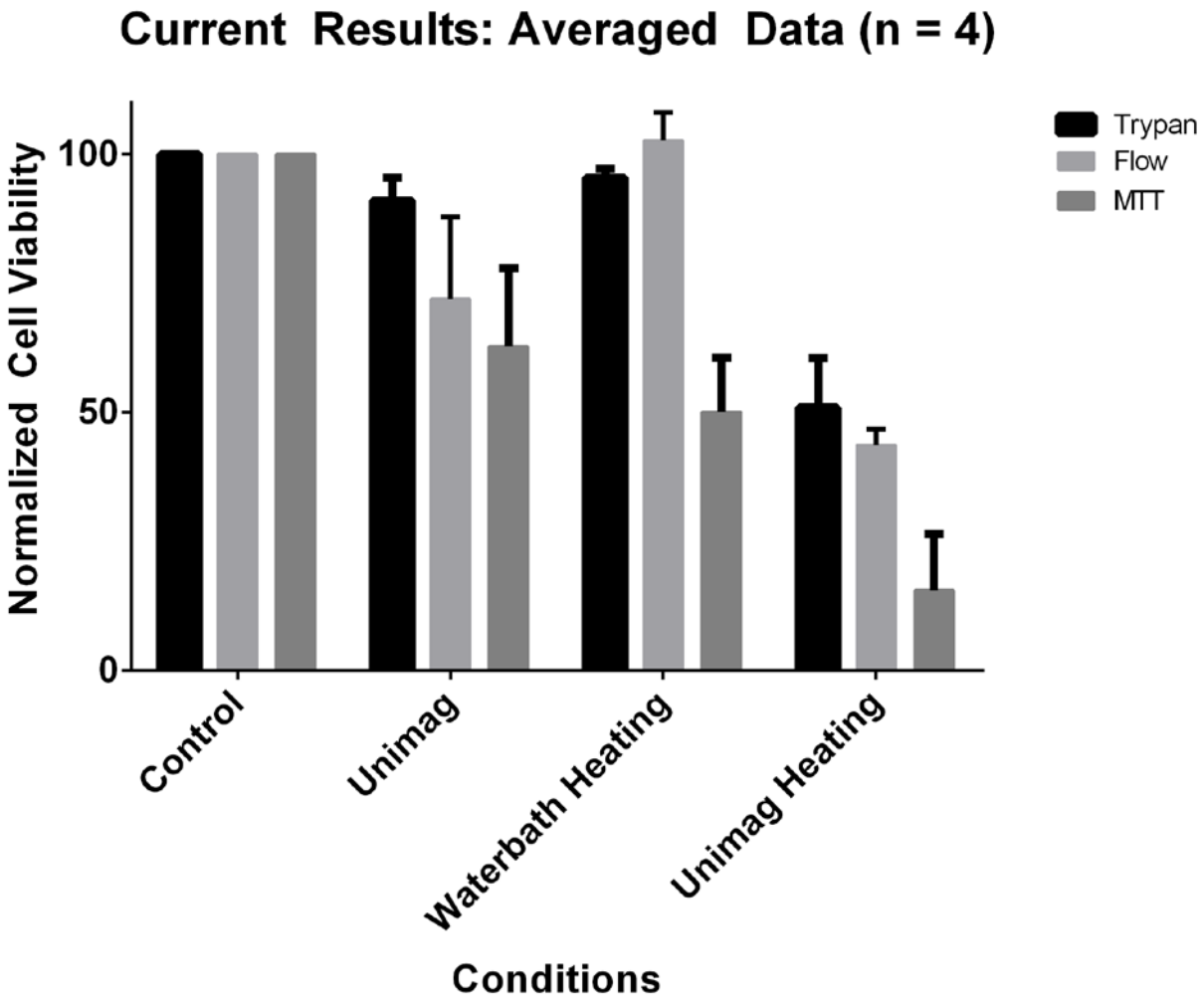

Figure 16: Summary of the final results from trypan blue exclusion method, annexin-V/PI flow cytometry, and MTT assay for comparison purposes.

Chapter 4

Discussion

In this study, the effect of the MNPs and hyperthermia on cellular permeability and integrity was evaluated by trypan blue exclusion via hemocytometer and annexin-V/PI affixation via flow cytometry, as seen in Figure 13 and Figure 14; both were investigated within one to three hours after treatment. These indicate that MH resulted in higher cell killing when compared to MNP exposure alone or conventional hyperthermia. On the other hand, considerable cell survivability was observed in conventional waterbath hyperthermia experiments. Typically, necrotic death occurs rapidly at temperatures above 46 °C; while at lower temperatures, apoptotic death occurs after several cell divisions after the initial treatment (Hildebrandt, et al., 2002; Van der Zee, 2002). Considering that the cell viability analysis were done within 1 – 3 hours of the treatment, these assays primarily portray the immediate effects on cell survivability due to MH. The control experiments with Unimag at this concentration without heating demonstrated some toxicity effects, but not enough to generate the significant differences between conventional and MH cell survival. There appears to be additional damage done to the plasma membrane of treated cells as a result of MH, which may be the outcome of cell membrane rupturing through mechanical vibrational damage under the influence of an AMF (Cheng, et al., 2014).

The extent of cellular membrane damage is determined by its ability to function as a gateway for the nutrients supporting the cell. Metabolized MTT salt product verifies the cell's capability to sustain reproductive ability and growth following exposure to the MNPs and heating. Once again, MH remained demonstrative of the highest level of cell killing when

compared to MNP exposure alone and to conventional hyperthermia, as seen in Figure 15. However, in this case, conventional hyperthermia exhibited a significant drop in cell survival in comparison to the results observed previously in the trypan blue exclusion and annexin-V/PI protocols as found in Figure 16. Despite the condition of the cellular membrane, the MTT assay measures for the cell's ability to metabolize, which provides a distinct measure for the survivability after treatment. Cytotoxic effects from the presence of the Unimag suspension remain noticeable at these concentrations; however, MH continues to exhibit an immense amount of cell killing aside from its interaction alone in the cell suspension.

In a similar study performed by Sadhukha et al. over a comparative study in the elimination of A549 (human lung adenocarcinoma) and MDA-MB-231 cells with conventional hyperthermia and MH, various cell viability assays were performed in order to investigate the effect of MH on cancer stem cells and its cell viability post-treatment. Conventional waterbath hyperthermia was conducted for 30 minutes at 46 °C. MH treatment involved the application of 2.5 mg Fe/mL MNPs with AMF strength and frequency of 6 kA/m and 386 kHz, respectively, for 5, 15, or 30 minute treatments. Maintained temperatures were between 43 and 46 °C after starting from thermal equilibrium at 37 °C. For comparative purposes, the average temperature for MH from that range is designated as 44.5 °C, which corresponds to $CEM_{43.0\ ^\circ C}$ = 85 minutes for the 30 minute treatment. Interestingly, conventional hyperthermia demonstrated a similar inadequacy in apoptotic death for A549 cells determined by annexin-V/PI assay through flow cytometry after 12 hours incubation with a normalized cell viability value of 96%. Considering that their waterbath heating was at 46 °C for only 30 minutes ($CEM_{43.0\ ^\circ C}$ = 240 minutes), the acquired normalized cell viability value of 102.61 ± 5.37% from my study with MDA-MB-231 cells appears to follow similar results for apoptotic death with this assay. For their 30 minute MH

result, a normalized cell viability value of 64% was determined, which also demonstrates a difference between the outcome of MH and conventional hyperthermia. Their clonogenic assay of the MDA-MB-231 cell line found a surviving fraction of approximately 50% and 0% for conventional hyperthermia and MH, respectively, after a 30 minute treatment (Sadhukha, et al., 2013). A comparison of my MTT assay results, as found in Figure 15, show similar, but slightly larger surviving fraction compared to the lack of colonies found by their study.

4.1 Cell Viability Assay

Determining the proper cell viability assay is essential for the interpretation of the cell killing response of any selected treatment. The gold-standard has been the clonogenic assay, which examines the ability to form colonies of cells after numerous divisions under extremely low initial cell seeding densities (Franken, et al., 2006). The primary disadvantage of this route consists of the required amount of days/weeks for a substantial number of colonies to grow. However, the clonogenic assay only addresses cell viability based on cells' proliferative ability, whereas novel techniques have been developed for a diverse set of interpretations of cell death in order to avoid the length of analysis time.

Trypan blue exclusion was used to detect the direct uptake of trypan blue dye based on cell membrane permeability, which has been depicted as an indicator for necrotic death due to the damaged holes present surrounding the cell (Strober, 1997). With average temperatures under 46 °C, apoptosis dominates over necrosis as the majority of the cell populations remain intact following hyperthermia. However, apoptosis can be challenging to determine solely under a microscope, which leads to our application of flow cytometry accompanied by annexin-V APC

and PI conjugates (Muppidi, et al., 2004). This flow protocol measures the cell integrity by distinguishing between early and late apoptotic death based on the presence of annexin-V alone or combined with PI, respectively. Healthy cells were cells with no annexin-V or PI attachment, whereas necrosis was established based on presence of PI alone. Supplementary flow cytometry averaged results can be found under the Appendix, section A.2. Despite a higher percentage of healthy cells when comparing the control and waterbath heating conditions, it was observed that late apoptotic markers increased by two-fold due to hyperthermia. This can be seen in the Unimag heating as well (see Figure 15).

Due to the lengthy process in the clonogenic assay, MTT assays have been used for its shorter time and cost to evaluate and unbiased analysis with instrumentation such as a plate reader. However, MTT assay results are highly sensitive to the preparation method and quality in reagents utilized, which calls for careful handling and precision (Nikzad & Hashemi, 2014). In a study performed by Zhang et al., MDA-MB-231 cells were induced with conventional hyperthermia at 43 °C for varying 10, 20, 30, 60, and 120 minute durations. MTT assay results reported normalized cell viabilities: 95%, 90%, 90%, 83%, and 68% in accordance to the above time points. They also performed clonogenic assays where normalized cell viabilities were reported as 94%, 99%, 85%, 62%, and 7%. Based on these results, it was concluded that the MTT assay may overestimate the cell viability when compared with the clonogenic assay (Zhang, et al., 2012). This seems to be consistent with our MTT results overestimating the cell viability; however, the severity after hyperthermia treatment after 120 minutes is not exactly captured in the MTT assay (68%) vs. the clonogenic assay (7%). Besides the difference in sensitivity from the MTT assay, similar outcomes are obtained due to comparable attributes that

the assays are identifying: the cell's ability to proliferate and grow based on its capacity to metabolize nutrients found in its surroundings/media even after being treated.

4.2 Magnetic Hyperthermia Parameters

The 5 kW induction power supply arrived pre-tuned to a 394 kHz frequency, in which the magnetic field strength could only be adjusted by varying the applied current. In order to fall within the biophysical limit for AMFs as designated by the critical product (Equation 2), the maximum magnetic field strength and frequency implemented for hyperthermia applications would then be set to 12.3 kA/m and 394 kHz, respectively. Since these parameters are appointed to its peak values, raising the field strengths or frequencies would induce intolerable conditions for human patients (Hergt & Dutz, 2007). Therefore the MNP properties and concentration are the primary variables in increasing temperatures.

In the pioneering MNP and lymph node deposition study performed by Gilchrist et al. in 1957, the author concluded that tolerable concentrations for MH were achieved, which are outlined in Figure 6. The iron concentration results demonstrate that roughly 70% of the excised dog lymph nodes contained at least 5.0 mg Fe/mL (Gilchrist, et al., 1957). The nodal cancer stage presents itself as a vital deciding factor for MNP concentrations based on the decreased space within the lymph node due to the presence of metastatic cells. However, by translating the information acquired by Wunderbaldinger et al., as found in Table 1, MNP iron concentrations for lymph nodes with the presence of metastatic cells were calculated to be around 3.0 mg Fe/mL (Wunderbaldinger, et al., 2002). The target application of using MH to control metastasis in the lymphatic system is to administer this treatment under cases when metastatic cells are present in

the lymph nodes. Under a conservative standpoint, MNP concentration of 3.0 mg Fe/mL was therefore selected in order to simulate feasible deposition of MNPs within micrometastatic lymph nodes.

Based on the regulation of temperatures by the body, accomplishing hyperthermic temperatures *in vivo* develops into a complex obstacle that is dependent on the rate of heat generation and its dissipation. Temperature monitoring of 1 mL milli-Q water without the AMF inside the constructed waterbath container, as represented in Figure 11, demonstrates the steady temperature of 37 °C surrounding the glass vial. Minimal temperature rise due to the effect of the AMF without MNPs presence was observed. The resulting MH temperature profile for *in vitro* heating, as shown in Figure 12, at maximum AMF parameters below the biophysical threshold critical product, succeeds in attaining hyperthermia temperatures (greater than 40°C) at an expedited rate; however, at the chosen concentration of 3.0 mg Fe/mL, AMF strength of 12.3 kA/m, and frequency of 394 kHz, an average temperature of 43.72 °C over an hour falls considerably below the potential heating at such high concentrations as found in other studies. In an *in vitro* MH study performed by Rodríguez-Luccioni et al., 42 – 45 °C was maintained over the course of two hours measurements with the following parameters: 0.6 mg Fe/mL of MNPs, an AMF strength of 20 kA/m, and frequency of 238 kHz (Rodríguez-Luccioni, et al., 2011). These heating experiments were conducted without the usage of a waterbath container providing a continuous flow of 37 °C, which explains the range of temperatures attained due to a lower concentration and AMF parameters. With the application of the waterbath container, a more accurate estimation of MH within a temperature regulating body is established in order to mimic its heating capacity *in vivo*.

4.3 Limitations of the Study

As reported, there appears to be minimal cytotoxic effects with the MDA-MB-231 cell line from Unimag MNPs at a concentration of 3.0 mg Fe/mL without any heating. Toxicity from the presence of nanoparticles is dependent on concentration as it will interact with the nutrients in cell culture medium and with the cell itself, potentially damaging and killing the cells. There exists a limited amount of studies that convey the concentrations of MNPs that reside into the lymph node post-injection, which hinders in the accuracy in determining feasible concentrations to apply with for MH. Selecting a concentration of 3.0 mg Fe/mL was based on data from only two studies, which leaves a fair bit of uncertainty in the actual concentration deposited in the lymph nodes. However, based on the nodal cancer stage, increased concentrations may not be possible for applications with metastatic cells present; meanwhile, decreased concentrations may not be a pertinent choice based on the maximum temperature of 44 °C reached with the AMF parameters at its limit. With regards to the heating rate of MNPs, the type of nanoparticle synthesis and suspension plays a substantial role in the potential of MH in lymph nodes.

Two possible alternative MNP suspensions were experimented with prior to selecting Unimag as the contender for the MH *in vitro* study. NanoXact 20 nm MNPs (NanoComposix, San Diego, CA) demonstrated excellent heating proficiency in milli-Q water; however, the suspension lost colloidal stability when diluted with cell culture medium rendering complete loss in heating capability. Sigma 10 nm MNPs (Sigma-Aldrich, St. Louis, MO) did not exhibit any type of heating in either milli-Q or cell culture medium, which was a result of its poor magnetic susceptibility based on synthesis techniques. Innovative Biomedical Technologies, Ltd. supplied Unimag nanoparticles for my studies as basis for a research collaboration between the company and the Ryerson University in efforts to yield favorable results towards heating lymph nodes

with MH. There are a limited number of studies involving the application of Unimag nanoparticles, especially *in vitro*. The lack of Unimag biocompatibility and cytotoxic data prevents the understanding in the potential toxicity effects found in suspensions with Unimag alone and no heating. However, it appears that its application has streamlined to clinical investigation for patients in Tbilisi, Georgia for SLN detection (Surguladze, 2010). Based on its projected applications in tissue, these nanoparticles have been fine-tuned with low Curie temperatures in order to improve the temperature control. Once the nanoparticles surpass the Curie temperature, the magnetic properties are released thus no longer being susceptible to the presence of AMFs (Cardarelli, 2008). This prospect leads to automatic regulation of temperature increase, which restricts the dissipation of heat past the boundaries of target region into healthy tissue (Astefanoaei, et al., 2016). This may be the possible reason behind the reduced heating rate once the average temperature has reached 44 °C as illustrated in Figure 12.

Chapter 5

Conclusions and Future Work

5.1 Summary and Conclusions

The *in vitro* lymph node model was designed taking account its geometric parameters, MNP concentrations feasible in a micrometastatic lymph node, and AMF parameters suitable for human patient use. The MDA-MB-231 human breast adenocarcinoma cell line was selected as a plausible candidate for drainage into the lymph nodes as metastatic cells. Four conditions were tested: control cells without heating, cells with the presence of Unimag MNPs, conventional waterbath heating, and MH. At a concentration of 3.0 mg Fe/mL MNPs and AMF parameters (12.3 kA/m, 394 kHz), an average temperature of 43.7 °C was maintained during a one hour treatment, in which normalized cell viability via trypan blue exclusion, annexin-V/PI flow cytometry, and MTT assay was evaluated as 50.9%, 43.6%, and 15.47%, respectively.

In conclusion, MH applied within a lymph node *in vitro* model demonstrated cell killing in the form of damaged plasma cell membrane and hindering the metabolic/proliferative function of MDA-MB-231 cells.

5.2 Future Work

The presented work serves as a precursor for *in vivo* studies using MH within a lymph node environment. Transitioning these methods into an *in vivo* model would be beneficial in determining the accuracy of the constructed *in vitro* lymph node model. Following the experimental design from *in vivo* studies for demonstrating MNP deposition inside animal lymph nodes (Gilchrist, et al., 1957; Wunderbaldinger, et al., 2002; Finas, et al., 2012) and clinical studies for profiling lymph node metastasis (Harisinghani, et al., 2007; Harada, et al., 2007; Johnson, et al., 2013), an investigation on the metastatic cell viability after the application of an AMF would determine the feasibility of administering MH within the lymphatic system. This would require the development of a considerably sized AMF system that could operate on various sizes of animals or human patients.

An interesting proposition, based on a premise by Cantillon-Murphy et al., would be to develop a system that could combine MRI and AMF mechanisms (Cantillon-Murphy, et al., 2010), which would enable metastasis detection and MH of the affected lymph nodes. However, the magnetic field strength for the MRI component would need to be decreased from the standard clinical strengths of 1.50 – 3.00 T to 0.35 T for the sole purpose in imaging lymph nodes, but at the same time, permit a second magnetic field to rotate MNPs in order to allow for heat generation from relaxational mechanisms. In the case where a combined MRI and MH system is implemented, introducing noninvasive temperature measurements by MR thermometry (Rieke & Pauly, 2008) would further demonstrate the versatility of the MH treatment modality in the lymphatic system.

Appendix

A.1 Nodal Cancer Stage Iron Concentration Calculations

The concentration of MNPs is derived from calculations based on data from Wunderbaldinger et al. Table 1 contains the final summary of the calculated values, which is based on a function of uptake percentage (*U*), injected dose (*ID*), and lymph node weight (W_L) (Wunderbaldinger, et al., 2002) as described in the equation below:

$$C_{Fe} = \frac{U \times ID}{W_L} \qquad [6]$$

with an injected dose of 10 mg Fe/kg [body weight] for a series of mice between 25 – 30 g, the reported uptake percentages and lymph node weights based on its nodal cancer stage can be found in Table 2, which implements the function found in Equation 6.

Table 2: Reported values for lymph node weight and uptake percentage based on the nodal cancer staging of the lymph node. Data obtained from (Wunderbaldinger, et al., 2002).

Nodal Cancer Stage	**Lymph Node Weight (mg)**	**Uptake Percentage (% ID/g)**
Normal Lymph Node	1.97 ± 0.21	8.60 ± 0.22
Micromestastatic	3.29 ± 1.14	4.2 ± 1.41
Small Metastases	5.96 ± 2.51	2.40 ± 0.71
Large Metastases	9.12 ± 3.78	0.96 ± 0.37

A.2 Flow Apoptosis Averaged Results

The following results were averaged based on the data collected from four separate annxein-V/PI flow cytometry experiments. Normalized cell viability results used in Figure 14 was calculated via utilizing the healthy category of no annexin-V and PI markers found on individual cells.

Table 3: Averaged results for annexin-V APC/PI flow cytometry protocol after heating for one hour with either conventional waterbath hyperthermia (44 °) or MH (3.0 mg Fe/mL, 12.3 kA/m, and 394 kHz).

Condition	**Healthy (AV-/PI-)**	**Early Apoptosis (AV+/PI-)**	**Late Apoptosis (AV+/PI+)**	**Necrosis (AV-/PI+)**
Control	73.2 ± 6.2%	21.3 ± 6.0%	5.5 ± 0.9%	0.0 ± 0.0%
Unimag	75.4 ± 9.8%	14.1 ± 7.7%	10.6 ± 2.2%	0.0 ± 0.1%
Waterbath Heating	53.3 ± 15.1%	32.5 ± 17.0%	14.0 ± 1.9%	0.2 ± 0.1%
Unimag Heating	32.0 ± 4.3%	40.5 ± 5.8%	27.4 ± 4.1%	0.1 ± 0.1%

References

Ahmed, M. & Douek, M., 2013. The Role of Magnetic Nanoparticles in the Localization and Treatment of Breast Cancer. *BioMed Research International,* Volume 2013, pp. 1-11.

Ahmed, M. & Douek, M., 2014. What is the Future of Magnetic Nanoparticles in the Axillary Management of Breast Cancer?. *Breast Cancer Res Treat,* Volume 143, pp. 213-218.

Asita, E. & Salehhuddin, H., 2013. Heat Sensitivity Between Human Normal Liver (WRL-68) and Breast Cancer (MDA-MB-231) Cell Lines. *International Journal of Chemical, Environmental & Biological Sciences (IJCEBS),* 1(1), pp. 191-195.

Astefanoaei, I., Dumitru, I., Chiriac, H. & Stancu, A., 2016. Thermfluid Analysis in Magnetic Hyperthermia Using Low Curie Temprature Particles. *IEEE Transactions on Magnetics,* 52(7), pp. 1-5.

Berry, C. C. & Curtis, A. S. G., 2003. Functionalisation of Magnetic Nanoparticles for Applications in Biomedicine. *Journal of Physics D: Applied Physics,* Volume 36, pp. 198-206.

Canadian Cancer Society, 2015. *Canadian Cancer Statistics (2015) - Special Topic: Predictions of the Future Burden of Cancer in Canada,* Toronto, ON: Canadian Cancer Statistics.

Cantillon-Murphy, P., Wald, L. L., Zahn, M. & Adalsteinsson, E., 2010. Proposing Magnetic Nanoparticle in Low-Field MRI. *Concepts in Magnetic Resonance Part A,* 36A(1), pp. 36-47.

Cardarelli, F., 2008. Magnetic Materials. In: *Materials Handbook: A Concise Desktop Reference.* Tuscon: Springer-Verlag London Limited, pp. 487-519.

Cheng, D., Li, X., Zhang, G. & Shi, H., 2014. Morphological Effect of Oscillating Magnetic Nanoparticles in Killing Tumor Cells. *Nano Express,* 9(195), pp. 1-9.

Chicheł, A., Skowronek, J., Kubaszewska, M. & Kanikowski, M., 2007. Hyperthermia - Description of a Method and a Review of Clinical Applications. *Reports of Practical Oncology & Radiotherapy,* 12(5), pp. 267-275.

Dutz, S. & Hergt, R., 2014. Magnetic Particle Hyperthermia - a Promising Tumour Therapy?. *Nanotechnology,* Volume 25, pp. 1-28.

Finas, D. et al., 2012. Distribution of Superparamagnetic Nanoparticles in Lymphatic Tissue for Sentinel Lymph Node Detection in Breast Cancer by Magnetic Particle Imaging. *Magnetic Particle Imaging,* Volume 140, pp. 187-191.

Franken, N. A. P. et al., 2006. Clonogenic Assay of Cells in vitro. *Nature Protocols,* 1(5), pp. 2315-2319.

Gilchrist, R. K. et al., 1957. Selective Inductive Heating of Lymph Nodes. *Annals of Surgery,* 146(4), pp. 596-606.

Giustini, A. J. et al., 2010. Magnetic Nanoparticle Hyperthermia in Cancer Treatment. *Nano Life,* Volume 1, pp. 1-23.

Hall, E. J. & Giaccia, A. J., 2012. Radiation Carcinogenesis. In: *Radiobiology for the Radiologist (7th Ed.).* Philadelphia, PA: LIPPINCOTT WILLIAMS & WILKINS, pp. 148-150.

Harada, T. et al., 2007. Evaluation of Lymph Node Metastases of Breast Cancer Using Ultrasmall Superparamagnetic Iron Oxide-Enhanced Magnetic Resonance Imaging. *European Journal of Radiology,* Volume 63, pp. 401-407.

Harisinghani, M., Ross, R. W., Guimaraes, A. R. & Weissleder, R., 2007. Utility of a New Bolus-Injectable Nanoparticle for Clinical Cancer Staging. *Neoplasia,* 9(12), pp. 1160-1165.

Hergt, R. et al., 1998. Physical Limits of Hyperthermia Using Magnetite Fine Particles. *IEEE Transactions on Magnetics,* 34(5), pp. 3745-3754.

Hergt, R. & Dutz, S., 2007. Magnetic Particle Hyperthermia - Biophysical Limitations of a Visionary Tumour Therapy. *Journal of Magnetism and Magnetic Materials,* Volume 311, pp. 187-192.

Hergt, R., Dutz, S. & Roder, M., 2008. Effects of Size Distribution on Hysteresis Losses of Magnetic Nanoparticles for Hyperthermia. *Journal of Physics: Condensed Matter,* Volume 20, pp. 1-12.

Hildebrandt, B. et al., 2002. The Cellular and Molecular Basis of Hyperthermia. *Critical Reviews in Oncology/Hematology,* Volume 43, pp. 33-56.

Huang, H. S. & Hainfeld, J. F., 2013. Intraveneous Magnetic Nanoparticle Cancer Hyperthermia. *International Journal of Nanomedicine,* Volume 8, pp. 2521-2532.

Huang, S. et al., 2012. On the Measurement Technique for Specific Absorption Rate of Nanoparticles in an Alternating Electromagnetic Field. *Measurement of Science and Technology,* Volume 23, pp. 1-6.

Jeyadevan, B., 2010. Present Status and Prospects of Magnetite Nanoparticles-Based Hyperthermia. *Journal of the Ceramic Society of Japan,* 118(6), pp. 491-401.

Johannsen, M. et al., 2007. Thermotherapy of Prostate Cancer Using Magnetic Nanoparticles: Feasibility, Imaging, and Three-Dimensional Temperature Distribution. *European Urology,* Volume 52, pp. 1653-1662.

Johnson, L., Charles-Edwards, G. & Douek, M., 2010. Nanoparticles in Sentinel Lymph Node Assessment in Breast Cancer. *Cancers,* Volume 2, pp. 1884-1894.

Johnson, L., Pinder, S. E. & Douek, M., 2013. Deposition of Superparamagnetic Iron-Oxide Nanoparticles in Axillary Sentinel Lymph Nodes Following Subcutaneous Injection. *Histophathology,* Volume 62, pp. 481-486.

Laurent, S., Dutz, S., Häfeli, U. O. & Mahmoudi, M., 2011. Magnetic Fluid Hyperthermia: Focus on Superparamagnetic Iron Oxide Nanoparticles. *Advances in Colloid and Interface Science,* Volume 166, pp. 8-23.

Lee, H. et al., 2014. Response of Breast Cancer Cells and Cancer Stem Cells to Metformin and Hyperthermia Alone or Combined. *PLOS ONE*, 9(2), pp. 1-11.

Maier-Hauff, K. et al., 2007. Intracranial Thermotherapy using Magnetic Nanoparticles Combined with External Beam Radiotherapy: Results of a Feasibility Study on Patients with Glioblastoma Multiforme. *Journal of Neuro-Oncology*, Volume 81, pp. 53-60.

Martini, F. H., Timmons, M. J. & Tallitsch, R. B., 2015. *Human Anatomy.* 8th ed. Illinois: Pearson Education, Inc.

Muppidi, J., Porter, M. & Siegel, R. M., 2004. Measurement of Apoptosis and Other Forms of Cell Death. In: *Current Protocols in Immunology.* s.l.:John Wiley & Son, Inc., pp. 3.17.1-3.17.36.

Nathanson, S. D., 2003. Insights into the Mechanisms of Lymph Node Metastasis. *Cancer,* 98(2), pp. 413-423.

Nikzad, S. & Hashemi, B., 2014. MTT Assay Instead of the Clonogenic Assay in Measuring the Response of Cells to Ionizing Radiation. *Journal of Radiobiology*, 1(1), pp. 3-8.

Noble, G., 2012. *Progress Report of Collaboration Ryerson University and Innovative Bio-medical Technologies Ltd,* Toronto: Ryerson University.

Okamoto, S., Olson, A. C., Berdel, W. E. & Vogler, W. R., 1988. Purging of Acute Myeloid Leukemic Cells by Ether Lipids and Hyperthermia. *Blood,* 72(5), pp. 1777-1783.

Pankhurst, Q. A., Connolly, J., Jones, S. K. & Dobson, J., 2003. Applications of Magnetic Nanoparticles in Biomedicine. *Journal of Physics D: Applied Physics,* Volume 36, pp. 167-181.

Pankhurst, Q. A., Thanh, N. T. K., Jones, S. K. & Dobson, J., 2009. Progress in Applications of Magnetic Nanoparticles in Biomedicine. *Journal of Physics D: Applied Physics,* Volume 42, pp. 1-15.

Pathak, A. P., Artemov, D., Neeman, M. & Bhujwalla, Z. M., 2006. Lymph Node Metastasis in Breast Cancer Xenografts is Associated with Increased Regions of Extravascular Drain, Lymphatic Vessel Area, and Invasive Phenotype. *Cancer Res*, 66(10), pp. 5151-5158.

Rieke, V. & Pauly, K. B., 2008. MR Thermometry. *Journal of Magnetic Resonance Imaging,* 27(2), pp. 376-390.

Riss, T. L. et al., 2004. Cell Viability Assays. *Assay Guidance Manual*, pp. 1-23.

Rodríguez-Luccioni, H. L. et al., 2011. Enhanced Reduction in Cell Viability by Hyperthermia Induced by Magnetic Nanoparticles. *International Journal of Nanomedicine,* Volume 6, pp. 373-380.

Rosensweig, R. E., 2002. Heating Magnetic Fluid with Alternating Magnetic Field. *Journal of Magnetism and Magnetic Materials,* Volume 252, pp. 370-374.

Sadhukha, T., Niu, L., Wiedmann, T. S. & Panyam, J., 2013. Effective Elimination of Cancer Stem Cells by Magnetic Hyperthermia. *Molecular Pharmaceutics,* Volume 10, pp. 1432-1441.

Sapareto, S. A. & Dewey, W. C., 1984. Thermal Dose Determination in Cancer Therapy. *International Journal of Radiation Oncology, Biology, Physics,* Volume 10, pp. 787-800.

Saraf, S., Ghosh, A., Kaur, C. D. & Saraf, S., 2011. Novel Modified Nanosystem Based Lymphatic Targeting. *Research Journal of Nanoscience and Nanotechnology,* 1(2), pp. 60-74.

Seegenschmiedt, M. H. & Vernon, C. C., 1995. A Historical Perspective on Hyperthermia in Oncology. In: *Thermoradiotherapy and Thermochemotherapy - Volume 1: Biology, Physiology, Physics.* Bernlin: Springer-Verlag, pp. 3-46.

Shao, Y. W., Khokha, R. & Hill, R. P., 2013. Tumor Progression and Metastasis. In: *The Basic Science of Oncology,*. New York: McGraw-Hill Education, LLC., pp. 219-242.

Shauer, A. J., Becker, W., Reiser, M. & Possinger, K., 2005. Definition of the Sentinel Lymph Node and Basic Principles of Detection. In: *The Sentinel Lymph Node Concept.* Berlin: Springer-Verlag, pp. 3-4.

Sleeman, J., Schmid, A. & Thiele, W., 2009. Tumor Lymphatics. *Seminars in Cancer Biology*, Volume 19, pp. 285-297.

Strober, W., 1997. Trypan Blue Exclusion Test of Cell Viability. In: *Current Protocols in Immunology.* s.l.:John Wiley & Sons, Inc., pp. A.eB.1-A.3B2.

Surguladze, B., 2010. *Diagnosis and Treatment Method of Malignant Tumours, and Marker Compounds.* Canada, Patent No. CA 2692570.

Surguladze, B., Zautashvili, Z. & Gelashvili, S., 2011. Novel Method of Detection of Sentinel Lymphatic Nodes in Malignant Tumors. *Journal of Innovative Medicine and Biology,* Volume 2, pp. 46-55.

Van der Zee, J., 2002. Heating the Patient: a Promising Approach?. *Annals of Oncology,* Volume 13, pp. 1173-1184.

Wunderbaldinger, P. et al., 2002. Detection of Lymph Node Metastases by Enhanced MRI in an Experimental Model. *Magnetic Resonance in Medicine,* Volume 47, pp. 292-297.

Zhang, R., Zhou, Y., Wang, P. C. & Sridhar, R., 2012. Evaluation of Tumor Cell Response to Hyperthermia with Bioluminescent Imaging. *J Basic Clin Med*, 1(1), pp. 16-19.